Science Bulletin 64 (2019) 1540–1556

Contents lists available at ScienceDirect

Science Bulletin

journal homepage: www.elsevier.com/locate/scib

Review

# Remote sensing of cyanobacterial blooms in inland waters: present knowledge and future challenges

Kun Shi [a,b,c], Yunlin Zhang [a,b,*], Boqiang Qin [a,b], Botian Zhou [d]

[a] Taihu Laboratory for Lake Ecosystem Research, State Key Laboratory of Lake Science and Environment, Nanjing Institute of Geography and Limnology, Chinese Academy of Sciences, Nanjing 210008, China
[b] University of Chinese Academy of Sciences, Beijing 100049, China
[c] Center for Excellence in Tibetan Plateau Earth Sciences, Chinese Academy of Sciences, Beijing 100101, China
[d] Chongqing Key Laboratory of Big Data and Intelligent Computing, Chongqing Institute of Green and Intelligent Technology, Chinese Academy of Sciences, Chongqing 400714, China

ARTICLE INFO

*Article history:*
Received 2 June 2019
Received in revised form 18 June 2019
Accepted 23 June 2019
Available online 2 July 2019

*Keywords:*
Cyanobacterial blooms
Inland waters
Bio-optical properties
Satellite
MODIS

ABSTRACT

Timely monitoring, detection and quantification of cyanobacterial blooms are especially important for controlling public health risks and understanding aquatic ecosystem dynamics. Due to the advantages of simultaneous data acquisition over large geographical areas and high temporal coverage, remote sensing strongly facilitates cyanobacterial bloom monitoring in inland waters. We provide a comprehensive review regarding cyanobacterial bloom remote sensing in inland waters including cyanobacterial optical characteristics, operational remote sensing algorithms of chlorophyll, phycocyanin and cyanobacterial bloom areas, and satellite imaging applications. We conclude that there have many significant progresses in the remote sensing algorithm of cyanobacterial pigments over the past 30 years. The band ratio algorithms in the red and near-infrared (NIR) spectral regions have great potential for the remote estimation of chlorophyll *a* in eutrophic and hypereutrophic inland waters, and the floating algae index (FAI) is the most widely used spectral index for detecting dense cyanobacterial blooms. Landsat, MODIS (Moderate Resolution Imaging Spectroradiometer) and MERIS (MEdium Resolution Imaging Spectrometer) are the most widely used products for monitoring the spatial and temporal dynamics of cyanobacteria in inland waters due to the appropriate temporal, spatial and spectral resolutions. Future work should primarily focus on the development of universal algorithms, remote retrievals of cyanobacterial blooms in oligotrophic waters, and the algorithm applicability to mapping phycocyanin at a large spatial-temporal scale. The applications of satellite images will greatly improve our understanding of the driving mechanism of cyanobacterial blooms by combining numerical and ecosystem dynamics models.



## 1. Introduction

On the Earth, inland waters are greatly important because they have numerous critical functions in the environment, despite covering only a relatively small area of the planet's surface [1]. Available inland water resources are emerging as a limiting factor in both quantity and quality for human development and ecological stability [2]. Inland waters provide critical and diverse habitats for a large amount of species and ecosystem services, which is indispensable for supporting biodiversity maintenance [2]. In addition, inland waters influence the climate system, as shown in general circulation models, and these waters form the essential components of the global hydrological, carbon and nutrient cycles [3–5]. However, with increasing human activities and climatic changes, inland waters have experienced unprecedented threats from the synergistic effects of multiple, co-occurring environmental stresses, including nutrient enrichment, inorganic and organic pollution, and global warming [6–10].

One of the severely disastrous consequences of these threats is the globally increasing frequency of cyanobacterial blooms in inland waters [11–13]. Mounting evidences show that cyanobacterial blooms have increased at a global scale in recent decades, and these blooms are highly likely to expand further owing to ongoing eutrophication, rising $CO_2$ concentration levels, and global warming in the future [14–18]. Cyanobacterial blooms can cause a series of serious environmental problems for inland waters and can severely stress the ecological structures, functions and aesthetics of aquatic ecosystems [19,20]. Specifically, blooms can decrease water clarity and therefore suppress submerged aquatic vegetation

* Corresponding author.
*E-mail address:* ylzhang@niglas.ac.cn (Y. Zhang).

https://doi.org/10.1016/j.scib.2019.07.002
2095-9273/

growth and populations [21,22]. The microbial degradation of cyanobacterial blooms may induce hypoxia resulting in the deaths of fish and benthic invertebrates [11,23]. Furthermore, cyanobacteria can produce a variety of toxins that result in liver, digestive, and neurological diseases when ingested by humans, fish and birds [24–26]. In summary, cyanobacterial blooms can pose a major threat to the use of aquatic ecosystems for drinking and irrigation water, fishing and recreational purposes. Obviously, timely monitoring, detection and quantification of cyanobacterial blooms are especially important for controlling public health risks and understanding aquatic ecosystem dynamics.

Routine methods for analyzing cyanobacterial biomass have been well documented through field sampling and laboratory analyses [19,27,28]. However, the traditional method is ill suited for monitoring a large number of inland waters at regional or national scales because cyanobacterial blooms generally exhibit strong variability. The traditional method is highly laborious, time-consuming, expensive, and it is practically impossible to obtain an overview of the spatial information on cyanobacterial blooms, which stops its application to the timely monitoring of cyanobacterial blooms at a large scale. Thus, there is a clear need for new approaches to facilitate the development of reliable and cost-effective monitoring programs for cyanobacterial blooms at local, regional, national, and global scales. Due to the advantages of simultaneous data acquisition over large geographical areas and with high temporal coverage, remote sensing strongly facilitates the monitoring of cyanobacterial blooms in inland waters [29–33].

Remote sensing technology has been widely used to investigate the biogeochemical constituents of inland waters, including total suspended matter (TSM) [34,35], chromophoric dissolved organic matter (CDOM) [36], particulate organic carbon (POC) [37], nutrients [38,39], trophic state index [40,41], submerged aquatic vegetation [21,42] and algae-associated indexes (such as chlorophyll-*a*, phycocyanin, cyanobacterial dominance, and algal bloom area) [30,43–47]. A bibliometric analysis shows that "hyperspectral", "ocean color", and "chlorophyll-*a*" are the three most commonly used keywords in SCI-indexed papers published between 1900 and 2018 regarding water color remote sensing and thus indicates that chlorophyll-*a* (Chl*a*) is one of the hotspots and cores of this field (Fig. 1). With the development of satellite instruments and available algorithms, remote sensing is evolving towards the routine use of cyanobacterial bloom monitoring [48–51]. Presently, most of the remote sensing methods developed for quantification of cyanobacterial biomass rely on algorithms aiming at Chl*a* and phycocyanin (PC) concentrations [43,44,52]. There are two types of characteristic pigment associated with cyanobacteria in inland waters [53–55].

For further application of remote sensing techniques to cyanobacterial bloom monitoring and research, an overview of the available state-of-the-art methods is demonstrated in this paper, the challenges and future directions are outlined based on recent publications, and the objective is to obtain a deeper insight into the problem and derive a basis for further improvements in this domain. The present review focuses on the optical properties of the cyanobacterial community, the algorithm development and validation for cyanobacterial bloom remote sensing, and the applications of multi-satellite data to cyanobacterial monitoring. This work partially complements the review of accomplishments in studies regarding inland water remote sensing [51,56–59].

(1) We conduct a comprehensive review of the optical properties of cyanobacterial communities covering various types of inland waters, including the absorption, specific absorption and remote sensing reflectance. This part provides the intrinsic physical basis for the development of cyanobacterial remote sensing algorithms and an explanation for challenges in constructing universal algorithms for inland waters.
(2) We perform a comparative analysis of bio-optical, semi-analytical and empirical algorithms specifically used to detect and quantify cyanobacterial pigments and blooms in various types of inland waters based on *in situ* measured remote sensing reflectance or multispectral satellite imagery. The advantages and limitations of these algorithms are discussed.

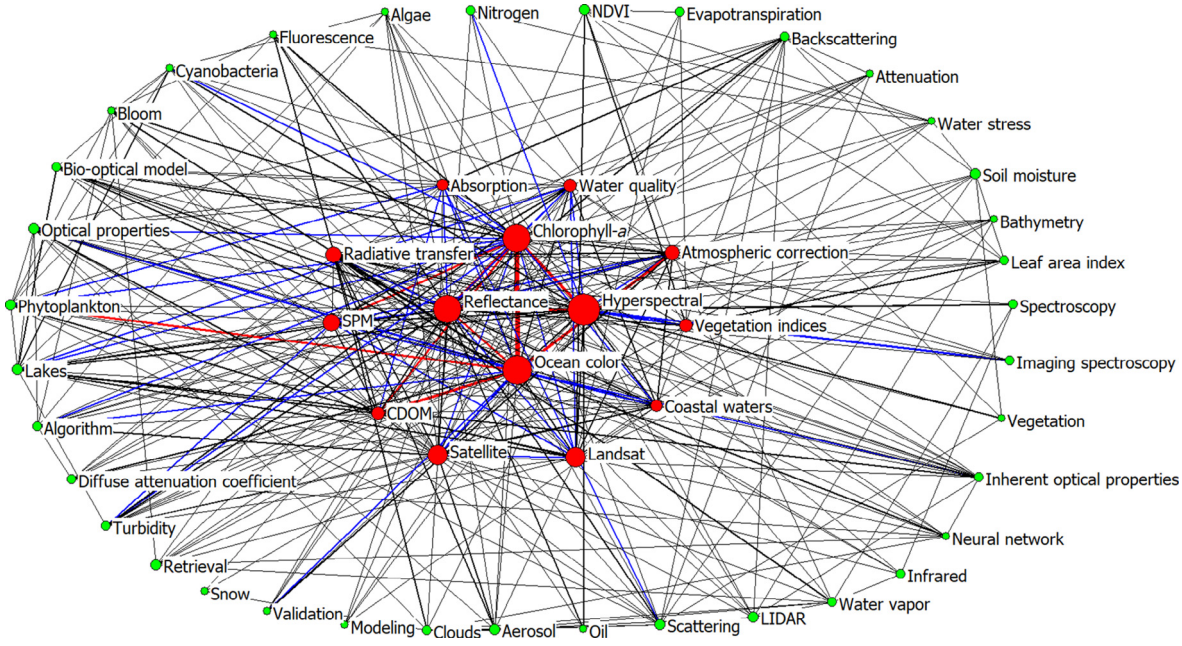


**Fig. 1.** Visualization of the relationships between the top 50 keywords used in the papers about water color remote sensing published between 1900 and 2018. The size of the circles proportionally represents the number of published papers. The color of the circles represents the frequency of keywords: red circles > 100 and aqua circles < 100; the color of the lines represents the number of co-occurrences: red lines > 30, blue lines > 15 but < 30 and black lines < 15.

(3) We discuss the application of MODIS, MERIS, GOCI, and Landsat data to the monitoring and mapping of cyanobacterial blooms over short and long-term periods and in local and regional water bodies. The roles of remote sensing techniques in lake management are addressed. We highlight the significant implications of satellite-derived cyanobacterial bloom dynamics at high temporal and spatial resolutions in addressing the impacts of climatic warming and eutrophication on cyanobacterial blooms.
(4) We conclude with the present challenges in algorithm development and remote sensing applications to the environmental management of inland waters and aquatic ecosystem research. Future research directions are proposed regarding the development of more accurate and transferable algorithms, the extension and application of remote sensing data and techniques in the research field of cyanobacterial blooms.

## 2. Overview of remote sensing of cyanobacterial blooms

Over the past several decades, cyanobacterial blooms remote sensing has made great progress, which is evidenced by a rapid increase in peer-reviewed publications on this study topic [56]. The ubiquitous phytoplankton pigment Chl*a* is generally considered an important indicator of cyanobacterial biomass, which can quickly respond to environmental changes [31]. This pigment exhibits a unique spectral characteristic with noticeable peaks in the blue (nearly at 440 nm) and red wavelengths (at nearly 675 nm), offering a physically theoretical basis for Chl*a* estimation from blue-to-green ratios of remote sensing reflectance in clear oceanic waters [33,60,61]. However, whereas Chl*a* in clear oceanic waters can be accurately derived based on the pigment's absorption peak in the blue band, the approach is sometimes unsuitable for inland waters due to the interference of CDOM and detritus particles in this spectral region [31–33]. In inland waters, many previous studies developed approaches to derive Chl*a* based on reflectance near Chl*a* absorption peak in the red and near-infrared (NIR) wavelength bands [30,31,62,63]. However, Chl*a* quantification is not the best way to accurately determine cyanobacterial abundance because this pigment exists in all phytoplankton communities. PC is a unique pigment of freshwater cyanobacteria that has a distinctive absorption feature at approximately 620–630 nm and is thus typically quantified using remote sensing data with a wavelength range of 615–630 nm [44,52,54,64–67].

Furthermore, the availability of algorithms for remotely deriving cyanobacterial biomass makes satellite quantification of cyanobacterial phenology possible [68,69]. Cyanobacteria can produce scums at the water surface in clam habitats because the bacteria can rapidly alter their buoyancy by regulating gas vesicles. The scums have optical characteristics that are similar to land vegetation [46]. Therefore, several land vegetation indexes, including the normalized difference vegetation index (NDVI), enhanced vegetation index (EVI), normalized difference peak-valley index (NDPI), visual cyanobacteria index (VCI) and floating algae index (FAI), were built to detect dense cyanobacterial blooms [47,50,70,71].

The long-term record of cyanobacterial blooms is crucial for developing management strategies, especially under the background of global warming and severe eutrophication, because it is often difficult to elucidate the causal factors of aquatic environmental changes without continuous and long-term water quality monitoring. The reliability of cyanobacterial biomass algorithms coupled with a large amount of multi-satellite data (MODIS/Landsat/MERIS) ensures the successful establishment of cyanobacterial bloom long-term historical records from remote sensing data [46,47,68,72]. The integration of satellite-derived long-term record products with *in situ* environmental and meteorological data has been used to clarify the cause and interrelationships between cyanobacterial dynamics (Chl*a*, PC, phenological index, and scums) and environmental and meteorological factors [30,46,48,68,73]. Climatic warming and eutrophication in global inland waters are potential drivers of cyanobacterial blooms [6,11].

## 3. Optical properties of the cyanobacterial community

Optical properties can be classified into two categories: inherent optical properties (IOPs) and apparent optical properties (AOPs). IOPs vary only with the composition and concentration of the medium or constituents and are independent of the ambient light field, such as absorption and scattering coefficients. AOPs not only depend on the composition and concentration of the medium or constituents but also on the ambient light field structure, such as remote sensing reflectance ($R_{rs}$) and various diffuse attenuation functions. The biological characteristics of cyanobacteria cause AOPs to interact with the light field through scattering and absorption processes and result in changes in the $R_{rs}$ of waters. Correspondingly, this physical connection is used to derive cyanobacteria biological information from $R_{rs}$. Presently, cyanobacteria remote sensing uses various algorithms that were developed through different optical characteristics, which mainly include absorption and fluorescence [31,74].

### 3.1. Absorption properties of cyanobacterial pigments

The spectral absorption coefficient of the cyanobacterial community determined by a spectrophotometer is the total absorption from Chl*a* and all other accessory pigments and is highly variable in shape (Fig. 2) [44,74–76]. Generally, the spectral absorption coefficient has two distinct absorption peaks at the blue (near 440 nm) and red wavelengths (near 670 nm) [77–79]. The absorption peak at the blue wavelength is due to the strong absorption by nearly all of the main pigments contained in the cyanobacterial cells. Compared with the absorption blue peak, the red peak is narrower and smaller, and this peak is primarily attributed to Chl*a* [75,80,81]. In addition, there is a less obvious peak at 620 nm, which is induced by PC [76,82,83].

The $a_{ph}(440)$ and $a_{ph}(675)$ collected from various lakes were reported to be in the ranges of 0.0004–455.32 and 0.0002–12.75 $m^{-1}$, respectively, and Chl*a* varied from 0.04 to 25,978.3 μg/L (Table S1 online). This finding indicated significantly large variations in $a_{ph}(\lambda)$ in inland waters. Generally, $a_{ph}(\lambda)$ increased with an increasing water trophic state index. For example, $a_{ph}(440)$ for the oligotrophic Lake Muttukad in India was less than 0.42 $m^{-1}$ for Chl*a* of 0.5–1.46 μg/L [84]. For the eutrophic Lake Taihu in China, $a_{ph}(440)$ and $a_{ph}(675)$ were from 0.09 to 32.50 $m^{-1}$ and from 0.03 to 9.44 $m^{-1}$, corresponding to Chl*a* of 4.0–448.9 μg/L [81]. For the extremely eutrophic Lake Hartbeespoort in South Africa with Chl*a* varying from 33 to 25,978.3 μg/L, $a_{ph}(440)$ could be up to 455.32 $m^{-1}$ [85]. These previous publications provide evidence that $a_{ph}(\lambda)$ not only varies across geographic regions but also within the same sites.

Specific absorption coefficients ($a^*_{ph}(\lambda)$) were generally defined simply as the ratio of $a_{ph}(\lambda)$ to Chl*a*, which can reflect the relationships between $a_{ph}(\lambda)$ and the cyanobacterial biomass [75,86]. In general, the Chl*a*-specific absorption coefficients $a^*_{ph}(440)$ and $a^*_{ph}(\sim675)$ were in the ranges of 0.0036–0.102 and 0.002–0.285 $m^2$/mg, respectively (Table S2 online). Specifically, $a^*_{ph}(\sim440)$ was higher than $a^*_{ph}(\sim675)$ in the eutrophic inland water. Taking Lake Taihu as an example, $a^*_{ph}(\sim440)$, ranging from 0.0051 to 0.0514 $m^2$/mg, was higher than $a^*_{ph}(\sim675)$, which ranged from 0.002 to 0.147 $m^2$/mg. Both $a^*_{ph}(\sim440)$ and $a^*_{ph}(\sim675)$ were

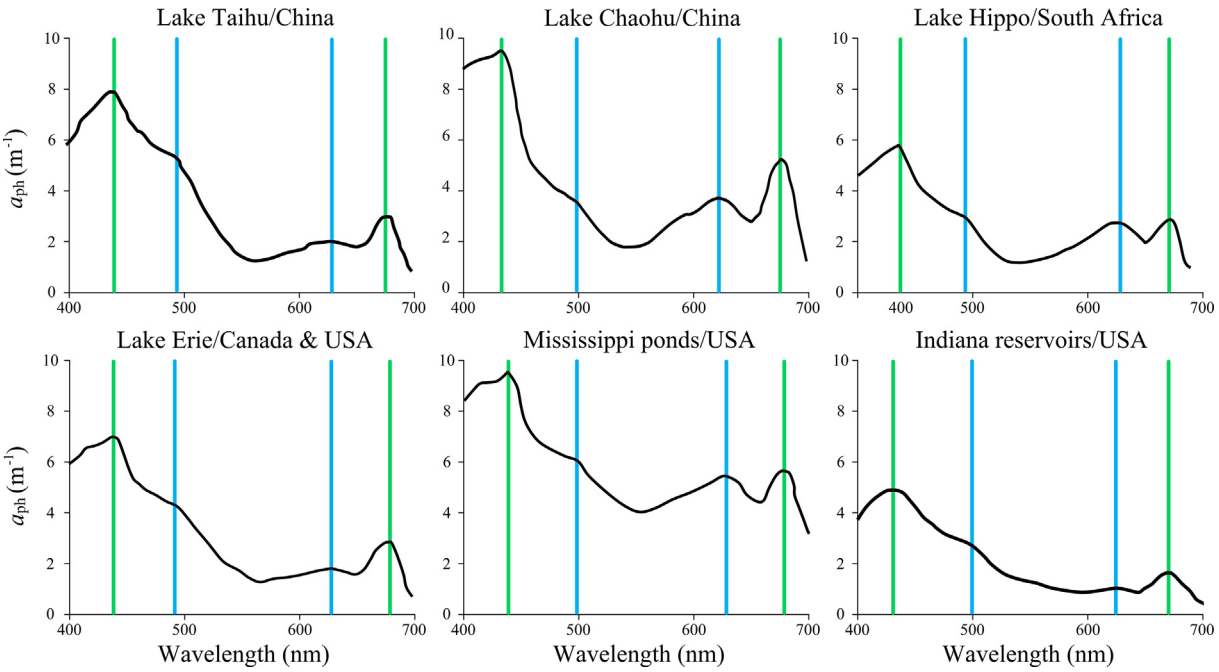


**Fig. 2.** Absorption spectra of cyanobacterial pigments measured from several inland lakes and reservoirs. The Chl*a* (vertical green lines at approximately 440 and 675 nm) and PC (vertical blue lines at approximately 500 and 620 nm) absorption peaks are shown [44,74–76].

negatively related to Chl*a* concentration (Fig. 3). The negative correlations between $a^*_{ph}(\lambda)$ and Chl*a* were also ascertained in previous studies [77,82,87,90,91].

Increased Chl*a* can be associated with an increase in intracellular pigment concentration rather than cell number, which causes an absorption efficiency loss in the package effect [92]. The pigment package leads to an absorption variation as cyanobacterial cells accumulate in the water column, and it has proven to be important to acclimate the cells to nutrient-rich, low-light conditions [93]. Fig. 3 demonstrates a more discrete $a^*_{ph}(440)$ compared to $a^*_{ph}(675)$ due to the low impact of the package effect on Chl*a*-specific absorption at the red peak. Moreover, the large change in $a^*_{ph}(440)$ and $a^*_{ph}(675)$ may be attributed to the accessory pigment variation, and the $a^*_{ph}(675)$ dynamics are reflected by different classes of cyanobacterial absorption spectral shapes (Fig. 3). There are significant variations in $a^*_{ph}(440)$ and $a^*_{ph}(675)$ for Chl*a* < 10 μg/L. Thus, the relationships between $a_{ph}(\lambda)$ and Chl*a* appear to be more variable in inland waters than in clean ocean waters. This variability in $a^*_{ph}(\lambda)$ must be considered in a bio-optical model using the relationships between $a_{ph}(\lambda)$ and Chl*a*. This large variability also indicates that the model based on cyanobacterial absorption for Chl*a* remote sensing is challenging.

As the diagnostic pigment of cyanobacteria, PC is practical in estimating cyanobacterial biomass. It is possible to further partition some of the main absorption coefficients based on decomposition algorithms. Several studies have determined that $a_{ph}(\lambda)$ can be decomposed into absorption coefficients of $a_{chla}(\lambda)$ and $a_{PC}(\lambda)$ [44,53]. In addition to determining $a^*_{ph}(\lambda)$, the algorithm can extract Chl*a* and determine the $a^*_{chla}(\lambda)$ by dividing the absorption spectra collected from the Chl*a* extraction by the independently quantified Chl*a* concentration. The $a^*_{PC}(\lambda)$ is determined by removing the absorption of Chl*a*, water, and particulate scattering at 620 nm from the $a^*_{ph}(\lambda)$ [54]. PC-specific absorption coefficient ($a^*_{PC}(620)$) was much weaker than $a^*_{chla}(620)$, which may be attributed to

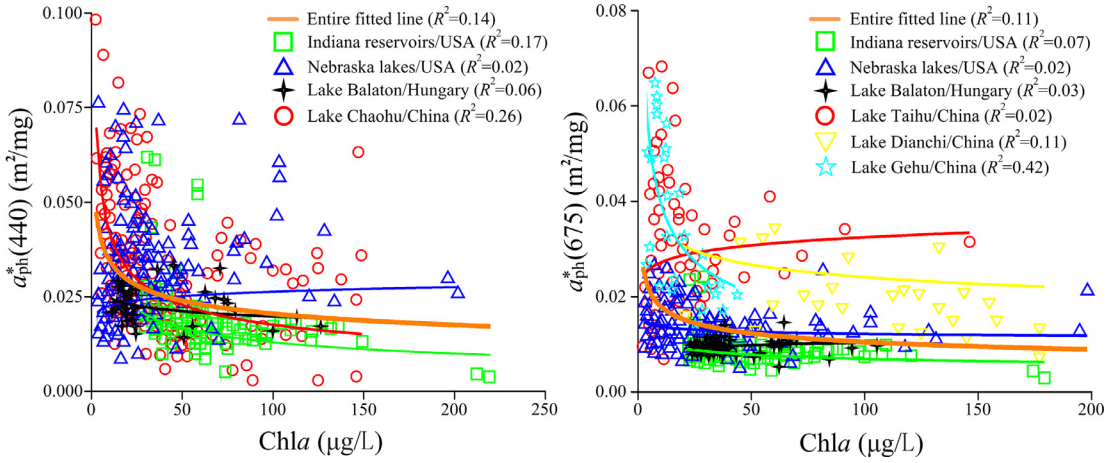


**Fig. 3.** Relationships between $a^*_{ph}(440)$, $a^*_{ph}(675)$, and Chl*a* concentrations of cyanobacterial blooms in a number of inland waters from previously published papers [82,87–89].

considerable noise when moving away from the PC absorption peak at approximately 620 nm [82]. The primary reason for the change in PC-specific absorption coefficients needs to be further elaborated through the controlled *in situ* and laboratory studies on the bio-optical properties of the cyanobacterial community.

### 3.2. Fluorescence properties of cyanobacterial pigments

Estimating phytoplankton pigments from the algal fluorescence signals of the photosystem that absorbs light for photosynthesis is based on the assumption that the pigments are proportional to the Chl*a* concentration [94]. For eukaryotic algae, most of the fluorescence (~95%) is emitted at approximately 685 nm and a longer wavelength range of 730–740 nm [95]. In contrast, most Chl*a* in cyanobacteria (beyond 70%) is contained in the photosystem and absorbs light, which fluoresces at wavelengths larger than 700 nm [96]. Recent studies have illustrated that the phycobilisomes of cyanobacteria possess varied, detectable fluorescence signals that overlap with the limited Chl*a* fluorescence emission of eukaryotic algae [97]. Consequently, a Chl*a* fluorescence peak is found near 680 nm in the cyanobacterial reflectance spectra, which is relatively lower than the reflectance at longer wavelengths towards the near-infrared bands, carrying amounts of spectral information that can be used to identify the specific fluorescence properties of Chl*a* [98].

With these findings as a starting point, fluorescence line height (FLH) was developed to measure the reflectance peak height near 680 nm caused by sun-induced Chl*a* fluorescence [99]. Furthermore, there is evidence that partial atmospheric corrections, accounting only for Rayleigh scattering and absorption, are more easily performed than aerosol corrections to demonstrate Chl*a* fluorescence signals from satellite spectroradiometers (e.g., MODIS, MERIS, and Ocean and Land Color Instrument (OLCI)) [30,100]. Therefore, the FLH algorithm does not depend on the full aerosol correction to provide a gross estimation of Chl*a* concentration and understand phytoplankton behavior in cyanobacteria-dominant inland waters with non-negligible near-infrared reflectance. However, the major light-harvesting antennae in cyanobacteria are phycobilisomes, including PC, phycoerythrin, and allophycocyanin (except for Chl*a*). Moreover, the FLH algorithm is significantly hampered by particulate and phytoplankton backscattering under high algae accumulate density and Chl*a* concentration (beyond 20 μg/L) [101]. Thus, from the perspective of inland waters where the scattering signal becomes dominant, the FLH algorithm based on sun-induced Chl*a* fluorescence is typically not the case for cyanobacteria, as previously explained.

Previous studies have shown that cyanobacteria containing PC can be distinguished using the linear correlation between the PC fluorescence and cyanobacterial biomass [96,97]. Other studies on the fluorescence properties of diagnostic pigments have also shown that PC is correlated with cyanobacterial biomass or microcystin concentration in aquatic ecosystems [102,103]. Consequently, the PC fluorescence emission of cyanobacteria has a considerably positive effect on the estimation of cyanobacterial pigments. Furthermore, the relationship between PC extraction efficiency and concentration is especially significant in diluted algal samples with a decreased PC/Chl*a* ratio, high light intensity, and low pigment fluorescence. In summary, we could further expect that fluorescence signals influenced by PC and Chl*a* can be used to distinguish cyanobacteria from other water constituents and estimate cyanobacterial biomass at both field and regional scales.

For fluorescence probes in quasi real-time cyanobacteria monitoring, there has been a widespread deployment of submerged fluorescence sensors for quantifying the diagnostic pigments of cyanobacterial blooms. In recent years, Chl*a* fluorescence parameters can be considered as proxies for the photosynthetic capacity of algal cells [104]. Specifically, the fluorescence ratio of $\Delta F/F_{m'}$, which represents the actual physiological activity, is taken as an algae viability assessment [105,106]. However, the actual fluorescent composition, uneven spectral distribution, and highly distinctive emission peaks derived from continuous photosynthetically active radiation in the 400–700 nm range are usually neglected in the phytoplankton communities of aquatic ecosystems. Moreover, pulse amplitude modulated (PAM) fluorometry is a prospective analytical technique that uses rapid and noninvasive indicators of photochemical efficiency in the phytoplankton communities [107]. Phyto-PAM fluorometry can separate cyanobacteria, green algae, and diatoms in terms of the fluorescence ratios derived from blue, green, and brown channels [108]. With respect to cyanobacteria detection, the PC fluorescence excitation at approximately 630 nm (brown channel) is extremely strong, while the Chl*a* fluorescence is hardly excited at 470 nm (blue channel) [109,110].

### 3.3. Remote sensing reflectance associated with the cyanobacterial community

For long-term monitoring of cyanobacterial bloom dynamics in a large water body, satellite sensor Chl*a* products are the most commonly used technical means. The MODIS Chl*a* standard product is suitable in inland waters with Chl*a* concentrations of up to 64 μg/L, and the upper limit of the MERIS product is 50 μg/L [111]. Conversely, *in situ* data suggest that the Chl*a* concentration of cyanobacterial blooms may be up to 1000 μg/L. The difference between satellite and *in situ* observations can be partially attributed to high reflectance in the near-infrared band, appearing spectrally to be terrestrial plants, which is not anticipated by the satellite-based water color algorithms [50,112]. These findings illustrate that remote sensing reflectance characteristics have not been clearly stated in applications to cyanobacterial community identifications.

Due to the influence of cyanobacteria floating on the water reflectance spectra for all phytoplankton species in cyanobacteria-dominant inland lakes and reservoirs, reflectance spectra may have one pair of double peaks (approximately 460 and 570 nm) and a valley between the double peaks (Fig. 4) [115]. In comparison, the unimodal peak between 400 and 600 nm is attributed to the strong Chl*a* absorption, which leads to low reflectance in the ranges of 400–500 nm and a reflectance minimum of approximately 625 nm.

As a crucial diagnostic pigment of the cyanobacterial community, PC is detectable by the secondary spectral characteristics in the reflectance spectra, with a reflectance peak near 640 nm [116]. There are many satellite sensor data containing the 640 nm wavelength where PC has an effect on the reflectance peak. However, an elevated cyanobacterial biomass may trigger deepening of the PC absorption peak at 620 nm. Thus, the simultaneous increase and decrease in the red reflectance (approximately 600–700 nm) will affect the stability of the PC reflectance characteristics derived from satellite multispectral images. Moreover, the 640 nm reflectance peaks measured from several inland waters in the UK and USA are located at longer wavelengths than those in the Asian lakes.

A visible scattering peak at 709 nm was concluded as the major reflectance characteristic of the cyanobacterial reflectance spectra in inland waters [117]. In extremely cyanobacteria-dominant waters, the 709 nm scattering peak shifts towards longer wavelengths due to strong pure water absorption that is minimized or excluded in the 700–750 nm waveband [118]. Although MERIS and Sentinel OLCI are the only frequently used satellite sensors with an appropriate band around the 709 nm reflectance peak,

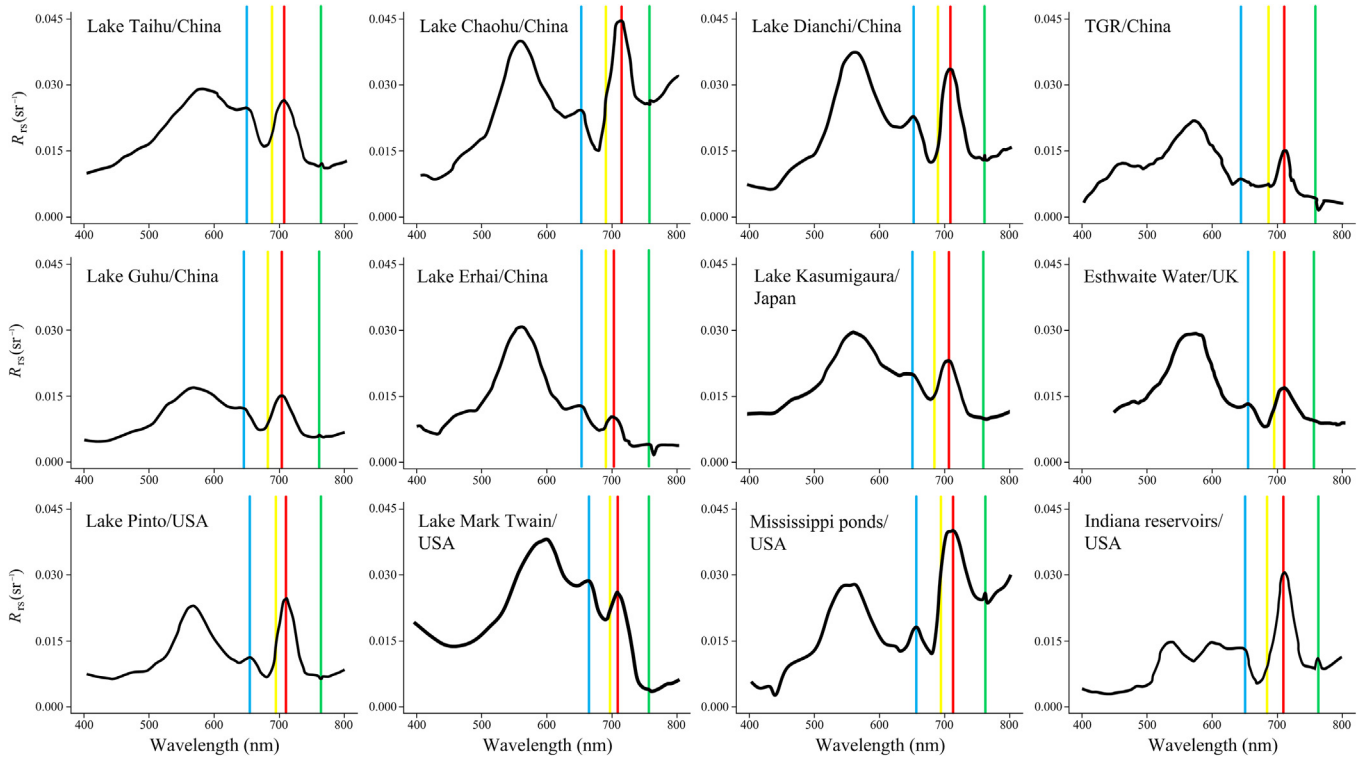


**Fig. 4.** *In situ* measured remote sensing reflectance spectra of cyanobacterial blooms with high Chl*a* concentrations in several inland lakes and reservoirs. The scattering (red) and fluorescence (yellow) peaks and PC (blue) and Chl*a* (green) reflectance peaks are shown [29,44,62,71,88,89,113,114].

different ratio-type algorithms, including 709 nm, have been used to accurately retrieve Chl*a* in inland waters [119,120]. In addition, the 709 nm peak height can be used as a proxy for determining whether blooms occur in highly productive waters because the red peak is thought to be due to the internal structure of the cyanobacterial community [71]. A narrower red peak in the 690–730 nm waveband can further represent low phytoplankton biomass in oligotrophic inland waters [33].

Surface scum in cyanobacterial blooms (Chl*a* concentration > 100 μg/L) can be identified when the 753 nm Chl*a* reflectance peak exceeds the 709 nm scattering peak [100]. Therefore, the distinctive reflectance peak at 753 nm is determined as an indicator for cyanobacterial community identification in surface scum conditions. The interference of adjacent floating vegetation can also be efficiently avoided using a 753 nm peak height threshold, and a short peak height at 753 nm may be caused by stray light [121].

## 4. Algorithms for cyanobacteria remote sensing

Algorithm development of cyanobacterial pigments has greatly progressed over the past 30 years. There is a wide variety of algorithms that can remotely quantify cyanobacterial biomass and blooms through Chl*a* or PC. The algorithms can be classified simply into three types: empirical, semi-empirical, and analytical approaches [32,122]. Empirical and semi-empirical approaches are usually developed with statistical relationships between $R_{rs}(\lambda)$ and cyanobacterial pigments (Chl*a* or PC). The difference between empirical and semi-empirical approaches is the assumptions used in the development of the approaches. The empirical approach completely relies on statistical techniques such as networks, least squares and stepwise regressions to build the best relationships between $R_{rs}(\lambda)$ and cyanobacterial pigments, without following any physical or optical principles of IOPs. The semi-empirical approach is usually based on a combination of $R_{rs}(\lambda)$ (three-band, band ratio, and so on.), and the selection of spectral bands follows certain physical or bio-optical principles. An analytical approach solves the physical equations of the radiative transfer models to derive the absorption coefficients of cyanobacterial pigments from $R_{rs}(\lambda)$.

### 4.1. Algorithms for Chla remote sensing

Empirical spectral band ratio algorithms are the most widely used for deriving Chl*a* in open ocean, coastal and inland waters [56]. Standard band ratio algorithms (OC2-OC4) for estimating Chl*a* in clean open oceans depend on the blue and green wavelength reflectance [123]. However, the blue-green band ratio algorithms are invalid for inland waters because the independent varying absorption of CDOM and TSM disturbs the correlation between the reflectance at these wavelengths and phytoplankton absorption [48,58,123]. The IOP and AOP characteristics of inland waters indicate that the reflectance in the red and NIR spectral regions has the potential to remotely derive Chl*a* in inland waters. The absorption peak in the red spectral regions is dominated by strong Chl*a* absorption but is minimally affected by CDOM and TSM [31,124]. Reflectance increases in the NIR spectral region due to the increased scattering from algal biomass, which is related to an increase in Chl*a* for most phytoplankton species [74,123]. To date, a large number of algorithms have taken advantage of these spectral indexes that are related to Chl*a* in the red and NIR spectral regions (Fig. 5) [29–31,46,74,75,81,88,99,113,120,123,125–131].

The band ratio algorithms have particular application potential to sensors with few bands, such as Landsat and MERIS. A model for deriving Chl*a* in Fremont Lakes State Recreation Area in Nebraska, USA, using the band ratio of band 7 and band 9 from MERIS data ($R^2$ = 0.94) showed that the simple MERIS band ratio model was slightly more accurate than the more complex models, with mean

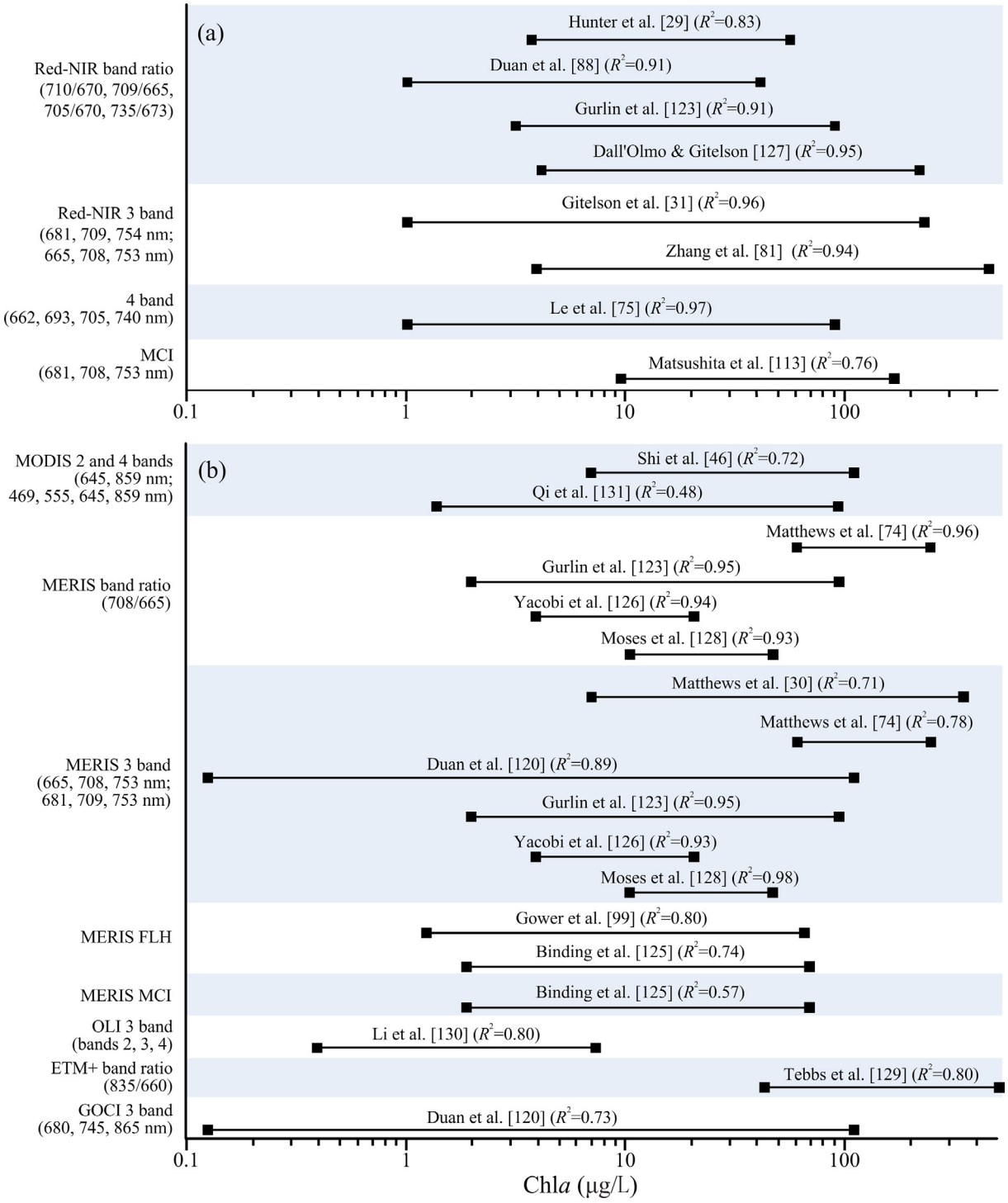


**Fig. 5.** Overview of previously published papers on Chl*a* retrievals from field spectral reflectance measurements (a) and a variety of satellite images (b) based on the band ratio algorithm, three-band algorithm, four-band algorithm, FLH algorithm, MHP algorithm and so on.

absolute errors of 2.3 μg/L for Chl*a* from 0 to 100 and 1.2 μg/L for Chl*a* from 0 to 25 μg/L [123]. Meanwhile, the band ratio algorithms utilizing MERIS satellite images in reservoirs of the Dnieper River (USA) showed that the relationship can be expressed as $Chla = 20R_{rs}(709)/R_{rs}(665) + 6.6$ ($R^2 = 0.93$) for Chl*a* from 10 to 40 μg/L [132]. Using the same spectral index, a model calibrated for small lakes in the Midwestern USA can well be used to estimate Chl*a* in subtropical Lake Kinneret (Israel) with a root mean square error (RMSE) of less than 1.5 μg/L ($Chla = 41R_{rs}(709)/R_{rs}(665) - 23.484$) for Chl*a* from 4 to 21 μg/L [126].

Several algorithms are partly based on the spectral band ratio index. To ensure the strength of the correlation between the reflectance band ratio and Chl*a*, an NIR band (754 nm) was subtracted from 709 to 665 nm [133]. However, this improvement does not work for turbid inland waters because the assumption that the NIR reflectance over water is mainly controlled by atmospheric effects is false over turbid inland waters. Instead of using a fixed NIR wavelength, some studies used a maximum reflectance peak height in NIR regions: $R_{rs}$(maximum reflectance peak)/$R_{rs}$(670) [59,113,124,134]. Following the bio-optical principle, the reflec-

tance band ratio in terms of absorption and backscattering coefficients of water constituents was reformulated to develop a semi-empirical model for Chl*a* extraction in inland and coastal waters [33,135]:

$$\mathrm{Chl}a = \frac{\left(\frac{R_{rs}^{-0}(\lambda_2)}{R_{rs}^{-0}(\lambda_1)}\right)(a_w(\lambda_2)+b_p) - a_w(\lambda_1) - b_p^c}{a_{ph}^*(\lambda_1)}, \quad (1)$$

where $R_{rs}^{-0}(\lambda_1)$ is the subsurface remote sensing reflectance at 672 nm, corresponding to the Chl*a* absorption peak in the red region; $R_{rs}^{-0}(\lambda_2)$ is the subsurface remote sensing reflectance at 704 nm; $b_p$ is the backscattering coefficient assumed to be independent of wavelengths; $a_w(\lambda_1)$ and $a_w(\lambda_2)$ are the absorption coefficients of pure water at 672 and 704 nm, respectively; $a_{ph}^*(\lambda_1)$ is the specific absorption of Chl*a* at 672 nm; and $c$ is a coefficient for improving the model performance and can be determined by the model regression fitting for datasets from several inland waters.

In addition, a simpler model is defined as follows [87]:

$$\mathrm{Chl}a = \frac{\frac{R_{rs}^{-0}(\lambda_2)}{R_{rs}^{-0}(\lambda_1)}a_w(\lambda_2) - a_w(\lambda_1)}{a_{ph}^*(\lambda_1)}, \quad (2)$$

where $R_{rs}^{-0}(\lambda_1)$ is the subsurface remote sensing reflectance at 665 nm, corresponding to the Chl*a* absorption peak in the red region; $R_{rs}^{-0}(\lambda_2)$ is the subsurface remote sensing reflectance at 708 nm; $a_w(\lambda_1)$ and $a_w(\lambda_2)$ are the absorption coefficients of pure water at 665 and 708 nm, respectively; and $a_{ph}^*(\lambda_1)$ is the specific absorption of Chl*a* at 665 nm.

Both algorithms make a number of assumptions [33,87,123,135]: (1) the water-leaving radiance in the red region is dominated by Chl*a* and pure water, and the influences of the remaining water constituents can be ignored; (2) compared to pure water, the absorption of the water constituents can be ignored in the NIR region; (3) the backscattering coefficients have very small variations with wavelengths; and (4) the specific absorption coefficient of Chl*a* in the red wavelengths is a constant for a specific type of water. Obviously, the two algorithms may be unreliable for deriving Chl*a* in the waters where optical properties are dominated by CDOM or TSM, although several studies have obtained promising results in their lake studies [88,136,137].

A more pronounced variation in the ratio is the three-band model, which can overcome the limitations of the above two algorithms. This model was originally developed for the extraction of Chl*a* concentrations of terrestrial vegetation [138]:

$$\mathrm{Chl}a \propto R_{rs}(\lambda_3)\left(\frac{1}{R_{rs}(\lambda_1)} - \frac{1}{R_{rs}(\lambda_2)}\right), \quad (3)$$

where $R_{rs}(\lambda_1)$ is the most sensitive to Chl*a* absorption, although the influences of other water constituents cannot be ignored; and $R_{rs}(\lambda_2)$ is minimally effected by Chl*a*. If the positions of $\lambda_1$ and $\lambda_2$ are as close as possible, the sensitivities of $R_{rs}(\lambda_1)$ and $R_{rs}(\lambda_2)$ to the presence of suspended sediments and CDOM are comparable and $\frac{1}{R_{rs}(\lambda_1)} - \frac{1}{R_{rs}(\lambda_2)}$ can remove the effects of the absorption of these water constituents. $R_{rs}(\lambda_3)$ is the least sensitive to absorption of Chl*a*, suspended sediments and CDOM and accounts for scattering [123]. The reflectance at $\lambda_3$ was introduced to remove the backscatter effects on estimation of Chl*a* [139]. The three-band model also has one important assumption that the changes in the backscattering coefficients at the three wavelengths are small enough to be ignored. The three-band model has been utilized to provide very good Chl*a* estimations in turbid and productive inland waters [59,126–128,132,139–141]. The optimal positions of each of the three wavelengths differ in different waters. The optimal wavelengths were determined to be $\lambda_1 = 670$ nm, $\lambda_2 = 710$ nm and $\lambda_3 = 740$ nm for Chl*a* from 2 to 180 μg/L [127]. The optimal three wavelengths were $\lambda_1 = 640$ nm, $\lambda_2 = 720$ nm and $\lambda_3 = 750$ nm for cyanobacteria-dominated waters for Chl*a* from 13.5 to 476.0 μg/L, but were $\lambda_1 = 685$ nm, $\lambda_2 = 700$ nm and $\lambda_3 = 730$ nm for the sediment-dominated waters for Chl*a* from 0.9 to 14.9 μg/L [139]. Adding an additional band to the three-band combination near 700 nm, a four-band algorithm was found to be an improvement over the three-band model in highly turbid lake water [139].

Several studies have shown that the Chl*a* fluorescence maximum near 685 nm is beneficial for deriving Chl*a* in inland waters [30,33,56,139,142]. The FLH algorithm is built using the fluorescence height, which is determined by a linear baseline drawn between two points on either side of the peak [30,33,99]:

$$\mathrm{FLH} = L2 - (L3 - L1)\frac{\lambda_2 - \lambda_1}{\lambda_3 - \lambda_1}, \quad (4)$$

where $L1$, $L2$ and $L3$ are the TOA radiances of waters at 760 ($\lambda_1$), 700 ($\lambda_2$) and 660 nm ($\lambda_3$), respectively. However, the FLH algorithm is only suitable for waters with relatively low biomass, which are generally Chl*a* < 30 μg/L. This is because the backscattering peak near 700 nm overwhelms the fluorescence peak in high-biomass water, and it is impossible to differentiate between the signal from particulate backscattering and solar-induced fluorescence in high-biomass waters [59]. A modified FLH algorithm has been developed, which is known as the maximum peak height (MPH) algorithm [30]. MPH tracks the position and magnitude of the maximum peak in the red/NIR spectral regions induced by either Chl*a* fluorescence or absorption/backscatter [65]. The red peak height is determined by the MPH with a constant baseline between 664 and 885 nm [30,79]. The MPH algorithm is proven to be better suited to high-biomass waters.

The analytical algorithm for Chl*a* estimation contains three key steps: solving the radiative transfer equation to derive the total backscattering and absorption coefficients from remote sensing reflectance at several wavelengths, parsing these coefficients into absorption coefficients of phytoplankton, and extracting Chl*a* from the absorption coefficient with the Chl*a*-specific coefficient [32,53,143,144]. However, the analytical algorithm is still not widely applied to inland waters for the following reasons. First, accurate remote sensing reflectance is a critical prerequisite for the successful application of the analytical algorithm to satellite data, which requires accurate atmospheric correction. It is still difficult to perform atmospheric corrections in turbid inland waters, particularly with blooms that can directly alter the remote sensing NIR region reflectance used in the correction. Therefore, uncertainties in the atmospheric correction greatly limit the algorithm application to inland waters. Second, specific IOPs play a vital role in the development of analytical algorithms, but the accurate quantification of Chl*a* based on IOPs remains a challenge in inland waters due to the large variations in Chl*a* specific absorption coefficients.

### 4.2. Algorithms for PC remote sensing

The remote estimation of PC is a challenging task due to a unique absorption spectral feature (absorption peak at ~620 nm) and low specific absorption coefficient [57]. By taking advantage of the PC absorption between ~615 and ~630 nm, there have already been several attempts to quantify PC based on empirical and semi-empirical methods [145]. Most algorithms use the spectral shape of the remote sensing reflectance and correlations between the reflectance band ratio and PC absorption [36,52,54,64,114,146–148].

The efforts in algorithm development and validation are summarized and depicted in Fig. 6 [24,29,44,52,54,55,64–67,88,114,116,137,149–151]. The empirical PC retrieval algorithms are generally established from statistical regressions between *in situ* measured PC and reflectance data observed by various optical

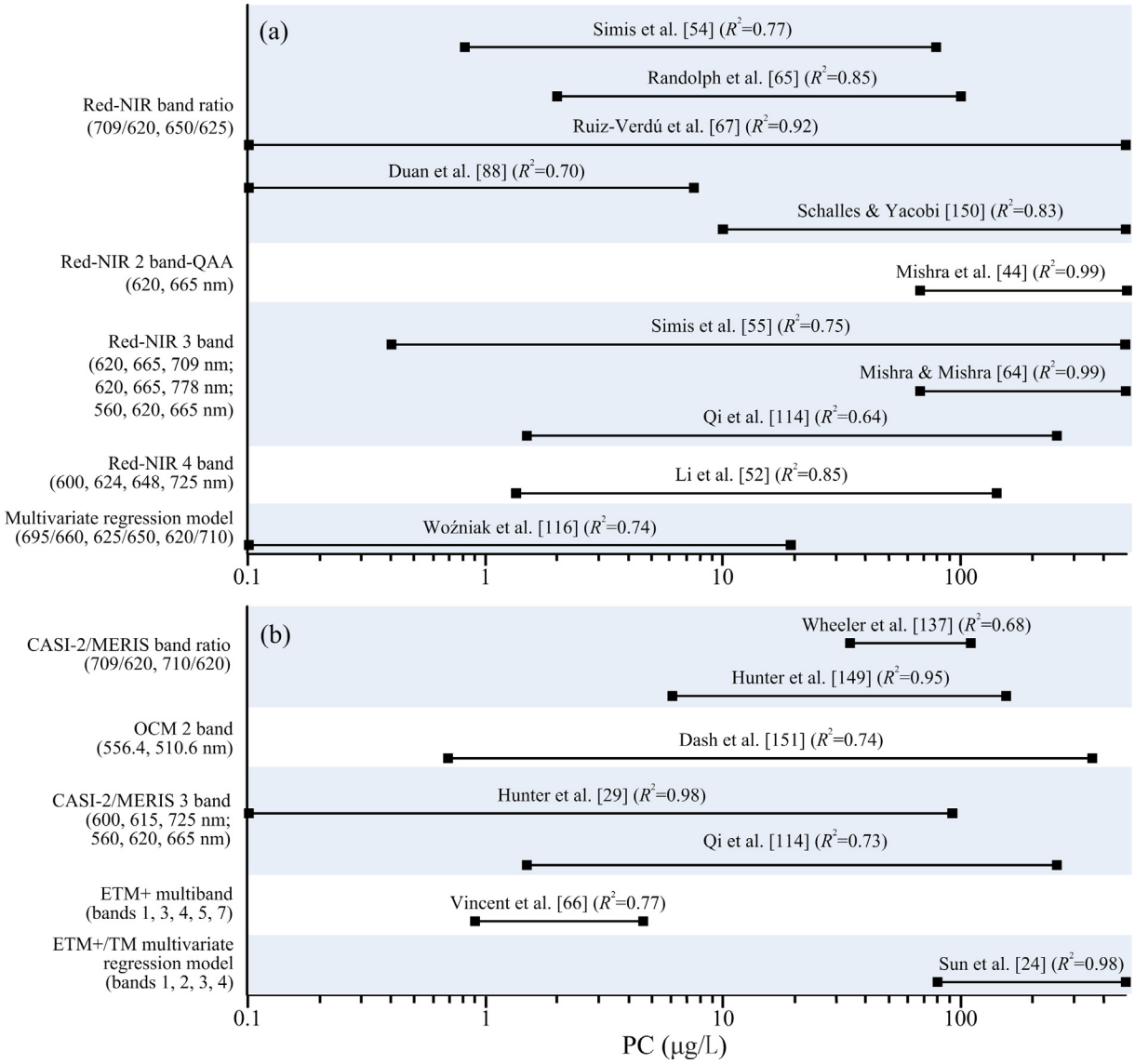


**Fig. 6.** Overview of previously published papers on PC retrievals from field spectral reflectance measurements (a) and a variety of satellite images (b).

satellite sensors [24,66,116,145,146,149]. Specifically, the single band (~620 nm) and band ratio, such as $R_{rs}(625)/R_{rs}(650)$ and $R_{rs}(595)/R_{rs}(660)$, are exploited in PC retrieval models [150]. In addition, a novel algorithm was developed using the ratio of water-leaving radiance at 710 and 620 nm from the Compact Airborne Spectrographic Imager (CASI) data for the Norfolk Broads in England ($R^2$ = 0.95) [149]. The normalized difference index using the 705 and 620 nm bands of MERIS and CHRIS was successfully derived PC [152]. However, the performance of these algorithms will be interfered if the absorption of Chl*a*, TSM and CDOM is high in inland waters. A MERIS or OLCI-based algorithm was established using multiple linear regression through two band ratio spectral indexes for PC from 0.05 to 18.95 μg/L ($R^2$ = 0.73; RMSE = 0.26 μg/L); the two band ratio spectral indexes are $R_{rs}(625)/R_{rs}(650)$ and $R_{rs}(620)/R_{rs}(710)$ [67,116]. Two empirical models were developed to quantify PC (from 1 to 5 μg/L) in Lake Erie with $R^2$ = 0.74 for the four-band model and $R^2$ = 0.78 for the band ratio model of Landsat 7 ETM+ (bands 1, 3, 5 and 7) [66]. In addition, some researchers have also shown that an empirical orthogonal function can be used to detect PC [147,153]. For example, based on Rayleigh-corrected reflectance at 469, 555, 645, and 859 nm from MODIS-Aqua data, a new approach was validated based on an empirical orthogonal function to quantify PC in Lake Chaohu, China ($R^2$ = 0.40) [147]. Recently, the empirical orthogonal function method using simulated MERIS or OLCI data resulted in RMSE = 0.29 μg/L for phycocyanin in productive waters [153]. However, these empirical orthogonal algorithms are often site-specific and need to be readjusted for applications to different sites or datasets [57].

A number of semi-empirical algorithms, including the three-band algorithm, nested band semi-empirical algorithm, derivative algorithm, and quasi-analytical algorithms, were recently proposed with the aim of overcoming the drawbacks of empirical algorithms [29,44,64,76,114,139,151]. Many researchers have semi-empirically derived PCs using the three-band algorithm. The form of the three-band algorithm for PC retrievals is the same as that for Chl*a*:

$$\mathrm{PC} \propto R_{rs}(\lambda_3)\left(\frac{1}{R_{rs}(\lambda_1)}-\frac{1}{R_{rs}(\lambda_2)}\right), \quad (5)$$

where $R_{rs}(\lambda_1)$ is the most sensitive to PC absorption, although the influences of other water constituents cannot be ignored; and $R_{rs}(\lambda_2)$ is the minimally affected by PC. $R_{rs}(\lambda_3)$ is the least sensitive

to the absorption of PC, TSM and CDOM and accounts for the scattering coefficients; for inland turbid waters, it is very important to introduce $R_{rs}(\lambda_3)$, which is used to further reduce the influence of absorption and scattering of the other water constituents. The spectral three-band index of $R_{rs}(750)[1/R_{rs}(630)-1/R_{rs}(660)]$ was well correlated with PC based on the laboratory experiment data [149]. Later, the three-band index to $R_{rs}(725)[1/R_{rs}(615)-1/R_{rs}(600)]$ was chanced using the data acquired by the Compact Airborne Spectrographic Imager-2 (CASI-2) and the Airborne Imaging Spectrometer for Applications (AISA) Eagle sensor for the two trophic and shallow lakes (Loch Leven and Esthwaite Water) ($R^2$ = 0.92 for 0 μg/L < PC < 93.7 μg/L) in the United Kingdom [29]. In highly turbid Lake Taihu, a four-band algorithm worked well in the PC estimation [139]:

$$\mathrm{PC} \propto \left(\frac{1}{R_{rs}(625)}-\frac{1}{R_{rs}(650)}\right)\left(\frac{1}{R_{rs}(730)}-\frac{1}{R_{rs}(695)}\right). \quad (6)$$

By introducing a correction coefficient ($\psi$) to reduce the influence of Chl*a* absorption, an improved three-band algorithm was built (Eq. (7)) [53]. The performance of this algorithm is much better than that of the traditional three-band algorithms [29].

$$\mathrm{PC} \propto R_{rs}(\lambda_3)\left(\frac{1}{R_{rs}(\lambda_1)}-\frac{1}{\psi R_{rs}(\lambda_2)}\right). \quad (7)$$

A combination of the three-band indexes and the baseline algorithm was used to remotely estimate PC for two reservoirs in Indiana, USA [52]:

$$\mathrm{PC}=208.3[[a_w(725)+b_b(725)](R31+R32)-2a_w(624)+a_w(600)+a_w(648)], \quad (8)$$

where $R31=R_{rs}(725)(\frac{1}{R_{rs}(624)}-\frac{1}{R_{rs}(600)})$; $R32=R_{rs}(725)(\frac{1}{R_{rs}(624)}-\frac{1}{R_{rs}(648)})$; $b_b(725)$ can be derived from remote sensing reflectance [141]; the band of 725 nm is selected to represent the backscattering effect; $R_{rs}(624)$ is the most sensitive to PC absorption; and $R_{rs}(600)$ and $R_{rs}(648)$ are used to reduce the effects of absorption and backscattering by other water constituents.

The derivative algorithms for PC remote detection were developed [114,151], which suggested that PC could be extracted from the remote sensing reflectance between 556 and 510 nm [151]. The researchers applied the algorithm to map PC in Lac des Allemands, Louisiana, USA, with Oceansat-1 satellite Ocean Color Monitor data. Based on the spectral band difference at approximately 620 nm (PCI), a PC retrieval model (Eq. (9)) was used to obtain PC temporal and spatial distributions in Lake Taihu and Lake Dianchi in China with MERIS images [114].

$$\mathrm{PC} \propto R_{rs}(560)+\frac{620-560}{665-560}[R_{rs}(665)-R_{rs}(560)]-R_{rs}(620). \quad (9)$$

In addition, the nested band semi-empirical algorithm based on the reflectance approximation and reflectance ratio of 709 and 620 nm to the PC absorption inverse at 620 nm ($a_{PC}(620)$) [54,55]:

$$\mathrm{PC}=\left[\frac{R_{rs}(709)}{R_{rs}(620)}[a_w(709)+b_b]-b_b-a_w(620)\right]^{1/\delta}-\varepsilon a_{ph}(665), \quad (10)$$

where $b_b$ is the spectrally invariant backscattering coefficient; $\delta$ is a correction coefficient that accounts for the assumption that absorptions by the rest of the water constituents, including Chl*a*, CDOM, and TSM, are small in the red regions; $\varepsilon$ is a conversion coefficient used to calculate the Chl*a* absorption coefficient at 620 from that at 665 nm; and $b_b$ can be derived from remote sensing reflectance [135]. PC could be derived by dividing $a_{PC}(620)$ by the specific absorption coefficient. This algorithm has received wide applications and has been proven to have great potential for PC estimations through validations in a number of studies in cyanobacterial-dominated inland waters [65,67,76,88]. This algorithm was improved by introducing the partition nonwater absorption coefficient into the contribution of non-PC pigments, CDOM and TSM to increase the estimation accuracy at low PC concentrations [76]. Other algorithms based on the quasi-analytical method were developed [44].

### 4.3. Approaches for remotely detecting dense cyanobacterial blooms

The dense cyanobacterial blooms have similar spectral reflectance characteristics to that of land vegetation, which exhibits very low values in the red region and noticeably high values in the NIR region with increasing Chl*a* concentration [47]. Thus, single band, band ratio and band difference have been used to remotely identify the dense cyanobacterial blooms in a similar manner as the vegetation detection [154–156]. The NDVI, the EVI, the normalized difference algae index (NDAI), the VCI, and the MERIS cyanobacterial index (CI) have been applied to various satellite data to identify dense cyanobacterial blooms in inland and coastal waters [157]. These spectral indexes are relatively simple and very easy to implement but sensitive to the performance of atmospheric correction due to aerosol type and thickness, sun glint, and solar viewing geometry. Furthermore, these algorithms also demonstrate significant variability in both the image background (water) and target (algal blooms) [158]. Thus, it is difficult to accurately derive information about dense cyanobacterial blooms using the above algorithms.

To overcome the disadvantages of these spectral indexes, a novel ocean color index FAI, was developed to detect floating algae using medium-resolution (250 and 500 m) data from the operational MODIS instrument, which has a definition similar to that of MODIS FLH and MERIS MCI [118] developed for Chl*a* estimation. Using the reflectance at 859 nm (vegetation "red edge") and a linear baseline between the red band (645 nm) and shortwave infrared band (1240 or 1640 nm), FAI is defined as follows [158]:

$$\mathrm{FAI}=R_{rc,NIR}-R'_{rc,NIR},$$

$$R'_{rc,NIR}=R_{rc,RED}+(R_{rc,SWIR}-R_{rc,RED})\frac{\lambda_{NIR}-\lambda_{RED}}{\lambda_{SWIR}-\lambda_{RED}}, \quad (11)$$

where $R'_{rc,NIR}$ is the baseline reflectance in the NIR band calculated from the linear interpolation between the red and SWIR bands; $\lambda_{RED}$, $\lambda_{NIR}$, and $\lambda_{SWIR}$ are selected as 645, 859 and 1240 nm, respectively; and $R_{rc,RED}$, $R_{rc,NIR}$ and $R_{rc,SWIR}$ are the Rayleigh-corrected reflectance at 645, 859 and 1240 nm, respectively.

FAI is nonsensitive to various atmospheric environments and observational conditions and is less influenced by the decreased absorption of water in the NIR region [50,154,157]. Thus, FAI is the most widely used spectral index for detecting dense cyanobacterial blooms in ocean, coastal and inland waters [46,59,70,112,159–161]. For example, long-term changes in the cyanobacterial bloom area in a number of lakes were derived using FAI, such as Lake Taihu [46,47,162–164], Lake Chaohu [73,161], Lake Dianchi [165,166] and Lake Erie [72]. Combined with other spectral indexes, FAI was also used to discriminate lake water, cyanobacteria blooms, submerged macrophytes, and emergent/floating macrophytes using MODIS imagery in large shallow and eutrophic inland water [160]. FAI is proposed based on MODIS data; however, FAI can also be applied with other satellite instruments, such as Landsat and AHI on Himawari-8 [70,72,159]. However, this algorithm needs to be further improved due to the following limitations: uncertainties in the total bloom coverage because algal mats can be smaller than the satellite pixel size and difficulty in more accurate estimations of threshold values for algae and nonalgae areas of optically complex eutrophic lakes.

Recently, several new algorithms have been developed to detect cyanobacterial blooms for inland waters, including the algae pixel-growing algorithm (APA) [154], the adjusted FAI (AFAI) [164] and baseline floating macroalgae height (VB-FAH) [167]. Replacing the input $R_{rc}(\lambda)$ in FAI with the top-of-atmosphere reflectance and discarding the center wavelengths in the calculation, an improved FAI algorithm called AFAI was developed using Landsat images [164]:

$$\mathrm{AFAI} = R_{rs,NIR} - R_{rs,RED} - 0.5(R_{rs,SWIR} - R_{rs,RED}), \quad (12)$$

where $R_{rs,RED}$, $R_{rs,NIR}$ and $R_{rs,SWIR}$ are the top-of-atmosphere reflectances in the red regions, NIR regions and SWIR regions, respectively. Compared to FAI, AFAI has several advantages [158,164]. First, the AFAI algorithm highlights the role of the reflected peak in the NIR region by reducing the difference between the NIR and SWIR, which would provide more prominent information on the cyanobacterial blooms. Second, discarding the center wavelengths in the FAI calculation can allow the computed results to be used with unlimited band information, so the AFAI could be applied to more satellite images. An application of AFAI was demonstrated to derive the temporal and spatial variability in cyanobacterial blooms in Lake Hulunhu (China) [168]. VB-FAH adopts the green and red bands as the baseline to measure the NIR reflectance height, which is defined as follows:

$$\mathrm{VB\text{-}FAH} = R_{rs,NIR} - R_{rs,Green} + (R_{rs,Green} - R_{rs,RED}) \times \frac{\lambda_{NIR} - \lambda_{Green}}{2\lambda_{NIR} - \lambda_{Green} - \lambda_{RED}}, \quad (13)$$

where $R_{rs,Green}$, $R_{rs,RED}$ and $R_{rs,NIR}$ are the reflectances in the green regions, red regions and NIR regions, respectively. The form of VB-FAH is similar to FAI, but the difference between them is the wavelength selections. VB-FAH can be ideally applied with Landsat-8/OLI, HJ-1/CCD, and GF-1/WFV spectral bands and is non-sensitive to interference from reflections and aerosols [167]. However, the major problem of this algorithm is the threshold determination to identify the bloom pixels and nonbloom pixels due to the mixed pixels and observation geometry; thus, a fixed threshold will be a compromise, which will lead to bloom area data deviation [165]. Based on FAI, a novel algorithm to estimate floating algae area at subpixel scales, denoted as APA, is developed and evaluated for a series of MODIS data [154]. This method first identifies seed pixels due to the pure algae endmember threshold and defines the algae coverage as 1.0. Then, the algal bloom coverage expands from the initial pure algae pixels or high-coverage pixels to low-coverage pixels, according to the relationship between adjacent pixels in a $3 \times 3$ pixel window. The APA approach serves as an objective and more accurate method to determine the bloom severity in both near real-time monitoring and historical analysis, thereby improving the capacity of decision makers to manage Lake Taihu and its basin [151].

## 5. Applications of satellite data to monitor cyanobacteria dynamics

Great progress has been made in water color algorithms as well as the products, technology and maturity of satellite sensors, which have demonstrated confidence in remotely sensed data with potential applications to water environmental management [32,58,59,158]. A variety of satellite data, such as Landsat, MODIS, MERIS, Sentinel OLCI, GOCI, Himawari-8 AHI, and NPP VIIRS, has been utilized to retrieve water quality in several oceans, coastal and inland waters [34,63,68,125,141,159,169–171]. Among these satellite data, Landsat, MODIS, MERIS and Sentinel OLCI are the most widely used for monitoring the spatial and temporal dynamics of cyanobacteria in inland waters due to their appropriate temporal, spatial and spectral resolutions.

### 5.1. Landsat series data

High spatial resolution (30 m) and long-time span (since the 1980s) give the Landsat series data the potential to obtain long-term cyanobacterial blooms dynamics in inland waters [24,50,66,72,129,130,172,173]. Several Landsat 8 OLI images with a bio-optical model were used to map temporal and spatial Chl*a* distributions from 2015 to 2017 in some deep subalpine lakes Northern Italy [173]. The results showed that Chl*a* would increase from 2 to 7 μg/L when cyanobacterial blooms began and dropped to initial value again within less than 20 d. A time series of remotely estimated Chl*a* from Landsat 8 OLI images was built between 2013 and 2015 and the relationship of Chl*a* to inflowing rate, rainfall, temperature, and sunshine duration was examined in Lake Qiandaohu (China) [130]. The potential of Landsat 8 OLI data was also evaluated with empirical models to determine Chl*a* in a tropical reservoir (Brazil) [174]. An empirical algorithm for Chl*a* estimation based on reflectance at bands 1–4 of Landsat TM and ETM+ was developed and then applied the proposed algorithm to the multi-temporal Landsat dataset to obtain Chl*a* time series between 2003 and 2010 for the Río Tercero reservoir (Argentina) [172]. The results showed that the maximum Chl*a* in the Río Tercero reservoir appeared in the spring of 2009 due to the high water surface temperature and rainfall; this study also observed higher Chl*a* values in branches of the western basin, which was explained by the higher nutrient availability generated by river inflows and the increase in water temperature resulting from the thermal effects of cooling water discharged into the reservoir [172].

The relationship between the FAI thresholds for classifying cyanobacterial blooms and VCI was established using Landsat ETM+ [50]. The application of the relationship of VCI classifications to three Landsat ETM+ images revealed that the volume of cyanobacterial blooms can be classified into the six VCI levels in Lakes Nishiura and Kitaura (Japan) [50]. Using 17 Landsat ETM + images and a band ratio model, Chl*a* time series and maps were presented during the period of Nov. 2003 to Feb. 2005 for a hypertrophic, saline-alkaline flamingo lake (Lake Bogoria in Kenya) [129]. The results demonstrated the advantages of Landsat ETM + in providing a synoptic view of cyanobacterial biomass in the lake and showed that the spatial variation in Chl*a* across this lake increases during the blooms immediately before the event disappears, while the spatial variation is relatively homogeneous at low Chl*a*. Cyanobacterial blooms estimated in the inland waters of North China based on Landsat series images demonstrated that the annual total frequencies of cyanobacterial blooms increased from 0 in 1982 to 11 times in 2016 [164]. Meanwhile, the effectiveness of Landsat data for detecting historical phytoplankton blooms in Lake Erie was evaluated using Landsat data from 1984 to 2001, which showed that the area of cyanobacterial bloom decreased in the late 1980s, stayed relatively low in the 1990s, and significantly increased thereafter [175]. The potential of using Landsat data to derive PC has been demonstrated in Lake Dianchi (China) [24] and Lake Erie [66]. However, Landsat's utility for monitoring the temporal variations in cyanobacteria is seriously limited by the long revisit cycle (16 d) and the wide band spectral resolution, especially in inland waters wherein rain and clouds are frequent or the cyanobacterial blooms change quickly, such as Lake Taihu and Lake Chaohu (China). Many algorithms of Chl*a* and PC remote estimations, such as three-band, four-band, FLH, MHP, MCI, and nested band semi-empirical algorithms, cannot be applied with Landsat series data to map cyanobacterial blooms due to the limited spectral information and low signal-to-noise ratios. In addition, no greater than 23 images can be provided by Landsat

for one year, which may be insufficient for accurately revealing the temporal characteristics of cyanobacterial bloom dynamics.

### 5.2. MODIS data

Having a short revisit time (two images/one day) and relatively high spatial resolution (250 m for the first two bands), MODIS can generate adequate spatial and temporal resolution for investigating long-term and short time variations in cyanobacterial blooms at large scales. Thus, MODIS data have attracted much attention from numerous researchers. These data are most popular to apply to observations of cyanobacterial blooms in Lake Taihu [46,47,112,147,154,162,163,176,177]. Monitoring the cyanobacterial blooms in this lake is significantly critical for water quality management. The 9-year MODIS time series data from 600 MODIS FAI products exhibited a significant increase in the annual frequency of cyanobacterial blooms from 2000–2004 to 2006–2008, when the blooms began earlier and had a longer duration [47]. The researchers also revealed that the most severe blooms in 2007 were due to conditions highly favorable for bloom development and proliferation. Using the same method, a number of studies have attempted to characterize the long-term trend of cyanobacterial blooms in Lake Taihu covering different time periods [46,154,162,163]. The MODIS observations from these studies concluded that the cyanobacterial bloom area exhibited an increasing trend across the entire lake, which is driven by a decrease in wind speed, climatic warming and high levels of nutrients [46,154].

An empirical model was developed and validated to generate a long-term Chl*a* from MODIS-Aqua observations from 2003 to 2013 in Lake Taihu, which then quantified the responses of cyanobacterial dynamics for nutrient enrichment and climatic conditions [46]. The results indicated that the sensitivity of cyanobacterial dynamics to climatic conditions varied by region, and temperature is the most important factor controlling Chl*a* interannual variability followed by phosphorus Lake Taihu. Recent study demonstrated that MODIS data have great potential for deriving the phenological information of cyanobacterial blooms [178]. Under climatic warming and high nutrients, a 29.9-d advancement of the cyanobacterial bloom initial date was observed in Lake Taihu from the available daily MODIS-Aqua data from 2003 to 2017 [178]. In addition to the traditional parameters related to cyanobacterial blooms, MODIS data also have some ability to derive the carbon in cyanobacteria and assess the status of cyanobacterial physiology in Lake Taihu [176]. For further application, the Chl*a* and PC derived from MODIS data can be used for cyanobacterial bloom risk mapping in eutrophic Lake Chaohu with a decision tree classification model [73], indicating that MODIS cyanobacterial risk mapping provides a new tool for reservoir and lake management programs.

Long-term variations in cyanobacterial biomass in the central basin of Lake Erie during June and July from 2003 to 2017 were remotely estimated from MODIS data [179]. The analysis of the long-time series CI showed that Lake Erie had a very low cumulative cyanobacterial biomass during August and September of 2003 to 2007, but the cumulative biomass has increased since 2008. Thus, continued monitoring of cyanobacteria using MODIS data was recommended to ensure safe drinking water for Lake Erie [179]. Discrimination of cyanobacterial blooms from other phytoplankton blooms and extraction of relative phycocyanin abundances in Lake Erie have successfully been performed using MODIS data, indicating that the data can provide a cost-effective practical screening method for the rapid detection and warning of potentially toxic cyanobacterial blooms in the lower Great Lakes [180]. An application of MODIS data utilizing the red and near-infrared bands was documented to derive Chl*a* from the MODIS imagery in Lake Erie [177]. A Chl*a* time series and area of cyanobacterial blooms for the period from July 2002 to December 2006 in Lake Tanganyika (Africa) was remotely derived from MODIS-Aqua data, suggesting that MODIS data allow improved detection of surface blooms in Lake Tanganyika [181].

Highly frequent observations give MODIS data great application potential in cyanobacterial bloom monitoring in of inland waters and in identifying the environmental driving factors for the long-term dynamics of cyanobacterial biomass. While the MODIS data have 36 spectral bands and high signal-to-noise ratios, nine spectral bands from 412 to 869 nm at approximately 1-km ground resolution designed for ocean color use and highly sensitive but with a narrow dynamic range are usually saturated most of the time over inland waters due to the turbid atmosphere and water [131]. Therefore, these bands cannot be used for monitoring cyanobacterial blooms. Only seven very limited spectral bands of 469, 555, 645, 859, 1240, 164 and 2130 nm designed for land use are useful for inland waters. Among these spectral bands, only 645 and 859 nm may be relatively sensitive to cyanobacterial biomass. Thus, MODIS data cannot provide very high accuracy in monitoring cyanobacterial blooms. The number of MODIS data applications to detect cyanobacterial bloom areas is much greater than that of Chl*a* in previous studies. Nearly no MODIS applications are found to extract PC in inland waters because the spectral band configuration does not allow for the detection absorption features caused by PC or any other spectral features that are characteristic of only cyanobacteria (lacking the 620 nm band).

### 5.3. MERIS/Sentinel 3 OLCI

MERIS data have a spatial resolution of 300 m (full resolution), a short revisiting time interval (2–3 d/image) and 15 spectral bands with sufficient signal-to-noise ratios over the full dynamic range [74,115]. Compared to other satellite instruments, MERIS data have more spectral bands (10 bands from 615 to 905 nm) in the spectral region corresponding to several reflectance characteristics that are usually used for remote estimations of Chl*a* and PC [125]. These sensor specifications ensure sufficient observational frequency and adequate sensitivity to enable viable change detection of cyanobacterial blooms in inland waters [182]. Recent studies have demonstrated MERIS as the optimal past sensor for providing detailed cyanobacterial bloom information products due to its radiometric, spectral, temporal, and spatial resolutions [74,114,118,123,126,128,133,182].

Several previous studies have demonstrated the application of MERIS data to accurately quantify Chl*a* and PC temporal and spatial patterns in various inland waters [30,114,169,171]. The application of MERIS data was performed to monitor the extensive surface slicks, thought to be Sargassum spp. in the Gulf of Mexico [118]. FLH index derived from the MERIS bands 7–9 was significantly and linearly correlated to Chl*a* concentration in eutrophic waters in the Laurentian Great Lakes [33]. However, using MERIS FLH to map Chl*a* in oligotrophic and mesotrophic areas of the Great Lakes remains problematic. In addition, the 708/664 band ratio algorithm derived from MERIS data was used to generate the Chl*a* spatial distribution in Zeekoevlei, a small hypereutrophic lake in South Africa [74]. The relationship between Chl*a* and environmental factors suggested that wind and waves were the dominant factors controlling the spatial variability and magnitudes of Chl*a* in this small lake. Several MERIS products were assessed in the Lake of the Woods, to confirm that MERIS MCI could identify cyanobacterial blooms [125]. This study provided evidence for the profound impact of wind mixing on Chl*a* detected by MERIS MCI. In addition, Chl*a* time series for the 50 largest South African water bodies between 2002 and 2012 from the MERIS using the MPH algorithm demonstrated a strong seasonal cycle with a Chl*a* peak during the summer [182]. The trend in the Chl*a* time series indicates that

overall eutrophication tended to be less severe in these water bodies between 2005 and 2011, and the spatial distribution showed that 62% of the 50 largest water bodies in South Africa were hypertrophic, with an average Chl*a* more than 30 μg/L. The researchers also indicated that the application of MERIS data to derive Chl*a* in oligotrophic and mesotrophic waters with Chl*a* less than 20 μg/L is the most challenging.

A total of 52 MERIS images covering the summers of 2004 to 2011 were utilized to map Chl*a* and cyanobacterial scum in the Curonian Lagoon, the largest lagoon in Europe, using two different band ratio algorithms [183]. Wind speed was identified as the main driving factor in the surface accumulation of cyanobacteria, as well as in the Chl*a* spatial distribution in the Curonian Lagoon. A normalized green-red difference index was applied to 325 MERIS scenes to analyze the long-term Chl*a* changes in Lake Poyang (China) [184]. The long-term Chl*a* distribution showed significant spatial and temporal variability in Chl*a,* but no significant trend was found for Chl*a* in Lake Poyang during the study period. Other researchers applied MERIS to derive PC products [55,137]. For example, the algorithms developed from the nested semi-analytical band ratio approach were validated based on MERIS data [54,55]. A long-term time series of PCs in Taihu Lake was successfully established from 535 MERIS FR images using the MERIS PCI algorithm, which showed both seasonal and interannual changes [114].

Unfortunately, MERIS ceased functioning in 2012. Subsequently, the European Space Agency developed a replacement: the OLCI. OLCI was launched onboard the space mission Sentinel-3A in February 2016 and has all the spectral channels of MERIS with a few additional channels [132]. Several recent studies have demonstrated that OLCI has the same suitability as MERIS in deriving cyanobacterial bloom information in inland waters [132,136]. In summary, MERIS has made a great contribution to observations of cyanobacterial blooms in inland waters on a global scale and at a high frequency. However, accurately monitoring cyanobacteria in waters with low Chl*a* using MERIS data remains challenging. With more spectral bands (21 bands) than MERIS, OLCI is expected to have more potential in cyanobacterial monitoring. Many Chl*a* and PC algorithms based on MERIS should be validated with OLCI data in future work.

## 6. Future challenges

Presently, we have gained many important findings and progresses; however, some critical challenges need to be resolved. First, the accuracy of Chl*a* estimation is severely limited by the high variations in $a^*_{ph}(\lambda)$ across various inland waters. The variability interferes with the relationships between $a_{ph}(\lambda)$ and Chl*a*, indicating that the use of algorithms based on cyanobacterial absorption for remote sensing of low Chl*a* is challenging. Therefore, more effort should be focused on how to remove the impacts of $a^*_{ph}(\lambda)$ on the algorithms. Second, it is still difficult to develop an algorithm that can be applied to derive cyanobacterial information in inland waters with complex optical properties, which has limited to generating standard Chl*a* product, similar to that in open ocean waters (MODIS OC3M or SeaWiFS OC4). While good performances of the band ratio and three-band algorithms are found in eutrophic and hypereutrophic waters, the parameters and optimal bands are significantly different in various inland waters. The use of the analytical algorithm is one way to address this challenge and thus should be given more attention. Third, the application of satellite images to map PC is seriously lacking. Most PC algorithms are developed using data acquired from field, ship or airborne hyperspectral sensors. Thus, the applicability of these algorithms to satellite images for mapping PC at a large spatiatemporal scale needs further improvement. Fourth, using satellite images for mapping cyanobacterial information in small inland waters is problematic. Currently, there is no suitable satellite instrument with high frequency that can accurately monitor cyanobacterial blooms in small inland waters. Generally, satellite images with simultaneously high temporal and spatial resolutions are not affordable for most long-term monitoring programs. Compared with satellite platforms, unmanned aerial vehicles (UAVs) can capture images at extremely high spatial and spectral resolutions (centimeters, hundreds bands) with high temporal frequencies (several times each day). Thus, we believe that UAVs can reasonably contribute to an improved understanding of cyanobacterial dynamics over space and time for small inland waters. Finally, the present satellite data application is limited to revealing the temporal and spatial distributions of cyanobacterial information. Future work should focus on extending applications to elucidate the driving mechanism of cyanobacterial blooms formation and predict cyanobacterial bloom occurrence by combining the numerical simulation and ecosystems dynamics models.

## Conflict of interest

The authors declare that they have no conflict of interest.

## Acknowledgments

This work was supported by the National Science and Technology Major Project of China (2017ZX07203001), the National Natural Science Foundation of China (41771472 and 41621002), the Youth Innovation Promotion Association of Chinese Academy of Sciences (2017365), the Key Research Program of Frontier Sciences of Chinese Academy of Sciences (QYZDB-SSW-DQC016), and the Strategic Priority Research Program of Chinese Academy of Sciences (XDA19070301).

## Author contributions

Kun Shi and Botian Zhou charted the figures and tables. Kun Shi, Yunlin Zhang, Boqiang Qin and Botian Zhou collected and analyzed the literatures. Kun Shi wrote the original draft. Yunlin Zhang and Boqiang Qin reviewed and edited the draft.

## Appendix A. Supplementary material

Supplementary material to this article can be found online at https://doi.org/10.1016/j.scib.2019.07.002.

## References

[1] Pekel JF, Cottam A, Gorelick N, et al. High-resolution mapping of global surface water and its long-term changes. Nature 2016;540:418.
[2] Corman J. Cleaner Chinese lakes. Nat Geosci 2017;10:469.
[3] Wik M, Varner RK, Anthony KW, et al. Climate-sensitive northern lakes and ponds are critical components of methane release. Nat Geosci 2016;9:99.
[4] Catalán N, Marcé R, Kothawala DN, et al. Organic carbon decomposition rates controlled by water retention time across inland waters. Nat Geosci 2016;9:501.
[5] Tong Y, Zhang W, Wang X, et al. Decline in Chinese lake phosphorus concentration accompanied by shift in sources since 2006. Nat Geosci 2017;10:507.
[6] Paerl HW, Huisman J. Blooms like it hot. Science 2008;320:57.
[7] Qin BQ, Xu PZ, Wu QL, et al. Environmental issues of Lake Taihu, China. Hydrobiologia 2007;581:3–14.
[8] van Vliet MTH, Flörke M, Wada Y. Quality matters for water scarcity. Nat Geosci 2017;10:800.
[9] Paerl HW, Paul VJ. Climate change: links to global expansion of harmful cyanobacteria. Water Res 2012;46:1349–63.
[10] Winslow LA, Leach TH, Rose KC. Global lake response to the recent warming hiatus. Environ Res Lett 2018;13:054005.
[11] Huisman J, Codd GA, Paerl HW, et al. Cyanobacterial blooms. Nat Rev Microbiol 2018;16:471–83.

[12] Carey CC, Ibelings BW, Hoffmann EP, et al. Eco-physiological adaptations that favour freshwater cyanobacteria in a changing climate. Water Res 2012;46:1394–407.
[13] Qin BQ, Paerl HW, Brookes JD, et al. Why Lake Taihu continues to be plagued with cyanobacterial blooms through 10 years (2007–2017) efforts. Sci Bull 2019;64:354–6.
[14] Johnk KD, Huisman J, Sharples J, et al. Summer heatwaves promote blooms of harmful cyanobacteria. Glob Change Biol 2008;14:495–512.
[15] Wagner C, Adrian R. Cyanobacteria dominance: quantifying the effects of climate change. Limnol Oceanogr 2009;54:2460–8.
[16] Kosten S, Huszar VLM, Becares E, et al. Warmer climates boost cyanobacterial dominance in shallow lakes. Glob Change Biol 2012;18:118–26.
[17] Michalak AM, Anderson EJ, Beletsky D, et al. Record-setting algal bloom in Lake Erie caused by agricultural and meteorological trends consistent with expected future conditions. Proc Natl Acad Sci USA 2013;110:6448–52.
[18] Taranu ZE, Gregory-Eaves I, Leavitt PR, et al. Acceleration of cyanobacterial dominance in north temperate-subarctic lakes during the anthropocene. Ecol Lett 2015;18:375–84.
[19] Paerl HW, Otten TG. Harmful cyanobacterial blooms: causes, consequences, and controls. Microb Ecol 2013;65:995–1010.
[20] Elliott JA. Is the future blue-green? A review of the current model predictions of how climate change could affect pelagic freshwater cyanobacteria. Water Res 2012;46:1364–71.
[21] Zhang YL, Jeppesen E, Liu XH, et al. Global loss of aquatic vegetation in lakes. Earth-Sci Rev 2017;173:259–65.
[22] Qin BQ, Gao G, Zhu GW, et al. Lake eutrophication and its ecosystem response. Sci Bull 2013;58:961–70.
[23] Juttner F, Watson SB. Biochemical and ecological control of geosmin and 2-methylisoborneol in source waters. Appl Environ Microb 2007;73:4395–406.
[24] Sun DY, Hu CM, Qiu ZF, et al. Estimating phycocyanin pigment concentration in productive inland waters using Landsat measurements: a case study in lake Dianchi. Opt Express 2015;23:3055–74.
[25] Merel S, Walker D, Chicana R, et al. State of knowledge and concerns on cyanobacterial blooms and cyanotoxins. Environ Int 2013;59:303–27.
[26] Carmichael WW. Health effects of toxin-producing cyanobacteria: "The cyanohabs". Hum Ecol Risk Assess 2001;7:1393–407.
[27] Qin BQ, Li W, Zhu GW, et al. Cyanobacterial bloom management through integrated monitoring and forecasting in large shallow eutrophic Lake Taihu (China). J Hazard Mater 2015;287:356–63.
[28] Xu H, Paerl HW, Qin BQ, et al. Nitrogen and phosphorus inputs control phytoplankton growth in eutrophic Lake Taihu, China. Limnol Oceanogr 2010;55:420–32.
[29] Hunter PD, Tyler AN, Carvalho L, et al. Hyperspectral remote sensing of cyanobacterial pigments as indicators for cell populations and toxins in eutrophic lakes. Remote Sens Environ 2010;114:2705–18.
[30] Matthews MW, Bernard S, Robertson L. An algorithm for detecting trophic status (chlorophyll-*a*), cyanobacterial-dominance, surface scums and floating vegetation in inland and coastal waters. Remote Sens Environ 2012;124:637–52.
[31] Gitelson AA, Dall'Olmo G, Moses W, et al. A simple semi-analytical model for remote estimation of chlorophyll-*a* in turbid waters: validation. Remote Sens Environ 2008;112:3582–93.
[32] Stumpf RP, Davis TW, Wynne TT, et al. Challenges for mapping cyanotoxin patterns from remote sensing of cyanobacteria. Harmful Algae 2016;54:160–73.
[33] Gons HJ, Auer MT, Effler SW. MERIS satellite chlorophyll mapping of oligotrophic and eutrophic waters in the Laurentian Great Lakes. Remote Sens Environ 2008;112:4098–106.
[34] Zhang YB, Zhang YL, Shi K, et al. A Landsat 8 OLI-based, semianalytical model for estimating the total suspended matter concentration in the slightly turbid Xin'anjiang reservoir (China). IEEE J-STARS 2017;9:398–413.
[35] Nechad B, Ruddick KG, Park Y. Calibration and validation of a generic multisensor algorithm for mapping of total suspended matter in turbid waters. Remote Sens Environ 2010;114:854–66.
[36] Kutser T, Pierson DC, Kallio KY, et al. Mapping lake CDOM by satellite remote sensing. Remote Sens Environ 2005;94:535–40.
[37] Duan HT, Feng L, Ma RH, et al. Variability of particulate organic carbon in inland waters observed from MODIS aqua imagery. Environ Res Lett 2014;9:084011.
[38] Song KS, Li L, Li S, et al. Hyperspectral remote sensing of total phosphorus (TP) in three central indiana water supply reservoirs. Water Air Soil Poll 2012;223:1481–502.
[39] Sun DY, Qiu Z, Li YM, et al. Detection of total phosphorus concentrations of turbid inland waters using a remote sensing method. Water Air Soil Poll 1953;2014:225.
[40] Wang SL, Li JS, Zhang B, et al. Trophic state assessment of global inland waters using a MODIS-derived forel-ule index. Remote Sens Environ 2018;217:444–60.
[41] Wen ZD, Song KS, Liu G, et al. Quantifying the trophic status of lakes using total light absorption of optically active components. Environ Pollut 2019;245:684–93.
[42] Han XX, Feng L, Hu CM, et al. Wetland changes of China's largest freshwater lake and their linkage with the three gorges dam. Remote Sens Environ 2018;204:799–811.
[43] Kutser T. Quantitative detection of chlorophyll in cyanobacterial blooms by satellite remote sensing. Limnol Oceanogr 2004;49:2179–89.
[44] Mishra S, Mishra DR, Lee Z, et al. Quantifying cyanobacterial phycocyanin concentration in turbid productive waters: a quasi-analytical approach. Remote Sens Environ 2013;133:141–51.
[45] Shi K, Zhang YL, Li YM, et al. Remote estimation of cyanobacteria-dominance in inland waters. Water Res 2015;68:217–26.
[46] Shi K, Zhang YL, Zhou YQ, et al. Long-term MODIS observations of cyanobacterial dynamics in Lake Taihu: responses to nutrient enrichment and meteorological factors. Sci Rep 2017;7:40326.
[47] Hu CM, Lee ZP, Ma RH, et al. Moderate Resolution Imaging Spectroradiometer (MODIS) observations of cyanobacteria blooms in Taihu Lake. China. J Geophys Res Oceans 2010:115.
[48] Odermatt D, Pomati F, Pitarch J, et al. MERIS observations of phytoplankton blooms in a stratified eutrophic lake. Remote Sens Environ 2012;126:232–9.
[49] Schaeffer BA, Bailey SW, Conmy RN, et al. Mobile device application for monitoring cyanobacteria harmful algal blooms using Sentinel-3 satellite ocean and land colour instruments. Environ Modell Softwa 2018;109:93–103.
[50] Oyama Y, Fukushima T, Matsushita B, et al. Monitoring levels of cyanobacterial blooms using the visual cyanobacteria index (VCI) and floating algae index (FAI). Int J Appl Earth Obs 2015;38:335–48.
[51] Palmer SCJ, Kutser T, Hunter PD. Remote sensing of inland waters: challenges, progress and future directions. Remote Sens Environ 2015;157:1–8.
[52] Li LH, Li L, Shi K, et al. A semi-analytical algorithm for remote estimation of phycocyanin in inland waters. Sci Total Environ 2012;435:141–50.
[53] Mishra S, Mishra DR, Lee Z. Bio-optical inversion in highly turbid and cyanobacteria-dominated waters. IEEE Trans Geosci Remote 2014;52:375–88.
[54] Simis SGH, Peters SWM, Gons HJ. Remote sensing of the cyanobacterial pigment phycocyanin in turbid inland water. Limnol Oceanogr 2005;50:237–45.
[55] Simis SGH, Ruiz-Verdu A, Dominguez-Gomez JA, et al. Influence of phytoplankton pigment composition on remote sensing of cyanobacterial biomass. Remote Sens Environ 2007;106:414–27.
[56] Blondeau-Patissier D, Gower JFR, Dekker AG, et al. A review of ocean color remote sensing methods and statistical techniques for the detection, mapping and analysis of phytoplankton blooms in coastal and open oceans. Prog Oceanogr 2014;123:123–44.
[57] Yan Y, Bao Z, Shao J. Phycocyanin concentration retrieval in inland waters: a comparative review of the remote sensing techniques and algorithms. J Great Lakes Res 2018;44:748–55.
[58] Odermatt D, Gitelson A, Brando VE, et al. Review of constituent retrieval in optically deep and complex waters from satellite imagery. Remote Sens Environ 2012;118:116–26.
[59] Matthews MW. A current review of empirical procedures of remote sensing in inland and near-coastal transitional waters. Int J Remote Sens 2011;32:6855–99.
[60] O'Reilly JE, Maritorena S, Mitchell BG, et al. Ocean color chlorophyll algorithms for SeaWiFS. J Geophys Res-Oceans 1998;103:24937–53.
[61] Brewin RJW, Raitsos DE, Dall'Olmo G, et al. Regional ocean-colour chlorophyll algorithms for the Red Sea. Remote Sens Environ 2015;165:64–85.
[62] Kudela RM, Palacios SL, Austerberry DC, et al. Application of hyperspectral remote sensing to cyanobacterial blooms in inland waters. Remote Sens Environ 2015;167:196–205.
[63] Duan HT, Zhang YC, Zhang B, et al. Estimation of chlorophyll-*a* concentration and trophic states for inland lakes in Northeast China from Landsat TM data and field spectral measurements. Int J Remote Sens 2008;29:767–86.
[64] Mishra S, Mishra DR. A novel remote sensing algorithm to quantify phycocyanin in cyanobacterial algal blooms. Environ Res Lett 2014;9:114003.
[65] Randolph K, Wilson J, Tedesco L, et al. Hyperspectral remote sensing of cyanobacteria in turbid productive water using optically active pigments, chlorophyll *a* and phycocyanin. Remote Sens Environ 2008;112:4009–19.
[66] Vincent RK, Qin X, McKay RML, et al. Phycocyanin detection from Landsat TM data for mapping cyanobacterial blooms in Lake Erie. Remote Sens Environ 2004;89:381–92.
[67] Ruiz-Verdú A, Simis SGH, Hoyos CD, et al. An evaluation of algorithms for the remote sensing of cyanobacterial biomass. Remote Sens Environ 2008;112:3996–4008.
[68] Palmer SCJ, Odermatt D, Hunter PD, et al. Satellite remote sensing of phytoplankton phenology in lake balaton using 10 years of MERIS observations. Remote Sens Environ 2015;158:441–52.
[69] Thackeray SJ, Jones ID, Maberly SC. Long-term change in the phenology of spring phytoplankton: species-specific responses to nutrient enrichment and climatic change. J Ecol 2008;96:523–35.
[70] Oyama Y, Matsushita B, Fukushima T. Distinguishing surface cyanobacterial blooms and aquatic macrophytes using landsat/TM and ETM + shortwave infrared bands. Remote Sens Environ 2015;157:35–47.
[71] Zhou B, Shang M, Wang G, et al. Distinguishing two phenotypes of blooms using the normalised difference peak-valley index (NDPI) and cyano-chlorophyta index (CCI). Sci Total Environ 2018;628–629:848.
[72] Chen J, He X, Zhou B, et al. Deriving colored dissolved organic matter absorption coefficient from ocean color with a neural quasi-analytical algorithm. J Geophys Res Oceans 2017;122:8543–56.
[73] Duan HT, Tao M, Loiselle SA, et al. MODIS observations of cyanobacterial risks in a eutrophic lake: implications for long-term safety evaluation in drinking-water source. Water Res 2017;122:455–70.

[74] Matthews MW, Bernard S, Winter K. Remote sensing of cyanobacteria-dominant algal blooms and water quality parameters in Zeekoevlei, a small hypertrophic lake, using MERIS. Remote Sens Environ 2010;114:2070–87.
[75] Le CF, Li YM, Zha Y, et al. Specific absorption coefficient and the phytoplankton package effect in Lake Taihu, China. Hydrobiologia 2009;619:27–37.
[76] Li LH, Li L, Song KS. Remote sensing of freshwater cyanobacteria: an extended iop inversion model of inland waters (IIMIW) for partitioning absorption coefficient and estimating phycocyanin. Remote Sens Environ 2015;157:9–23.
[77] Xue K, Zhang YC, Duan HT, et al. Variability of light absorption properties in optically complex inland waters of Lake Chaohu, China. J Great Lakes Res 2017;43:17–31.
[78] Simis SGH, Kauko HM. *In vivo* mass-specific absorption spectra of phycobilipigments through selective bleaching. Limnol Oceanogr-Meth 2012;10:214–26.
[79] Suslin V, Churilova T. A regional algorithm for separating light absorption by chlorophyll-*a* and coloured detrital matter in the black sea, using 480–560 nm bands from ocean colour scanners. Int J Remote Sens 2016;37:4380–400.
[80] Lorenzoni L, Toro-Farmer G, Varela R, et al. Characterization of phytoplankton variability in the cariaco basin using spectral absorption, taxonomic and pigment data. Remote Sens Environ 2015;167:259–68.
[81] Zhang YL, Liu ML, Qin BQ, et al. Modeling remote-sensing reflectance and retrieving chlorophyll-*a* concentration in extremely turbid case-2 waters (Lake Taihu, China). IEEE Trans Geosci Remote 2009;47:1937–48.
[82] Nguy-Robertson A, Lin L, Tedesco LP, et al. Determination of absorption coefficients for chlorophyll *a*, phycocyanin, mineral matter and cdom from three central Indiana reservoirs. J Great Lakes Res 2013;39:151–60.
[83] Yacobi YZ, Köhler J, Leunert F, et al. Phycocyanin-specific absorption coefficient: eliminating the effect of chlorophylls absorption. Limnol Oceanogr-Meth 2015;13:157–68.
[84] Simon A, Shanmugam P. Estimation of the spectral diffuse attenuation coefficient of downwelling irradiance in inland and coastal waters from hyperspectral remote sensing data: validation with experimental data. Int J Appl Earth Obs 2016;49:117–25.
[85] Matthews MW, Bernard S. Characterizing the absorption properties for remote sensing of three small optically-diverse south African reservoirs. Remote Sens 2013;5:4370–404.
[86] Binding CE, Jerome JH, Bukata RP, et al. Spectral absorption properties of dissolved and particulate matter in Lake Erie. Remote Sens Environ 2008;112:1702–11.
[87] Gilerson AA, Gitelson AA, Zhou J, et al. Algorithms for remote estimation of chlorophyll-*a* in coastal and inland waters using red and near infrared bands. Opt Express 2010;18:24109–25.
[88] Duan HT, Ma RH, Hu CM. Evaluation of remote sensing algorithms for cyanobacterial pigment retrievals during spring bloom formation in several lakes of East China. Remote Sens Environ 2012;126:126–35.
[89] Xue K, Zhang YC, Ma RH, et al. An approach to correct the effects of phytoplankton vertical nonuniform distribution on remote sensing reflectance of cyanobacterial bloom waters. Limnol Oceanogr-Meth 2017;15:302–19.
[90] Riddick CAL, Hunter PD, Tyler AN, et al. Spatial variability of absorption coefficients over a biogeochemical gradient in a large and optically complex shallow lake. J Geophys Res-Oceans 2015;120:7040–66.
[91] Shi K, Li YM, Lin L, et al. Absorption characteristics of optically complex inland waters: implications for water optical classification. J Geophys Res-Biogeosci 2013;118:860–74.
[92] Bricaud A, Babin M, More A, et al. Variability of chlorophyll specific absorption coefficient of natural phytoplankton analysis and parameterize. J Geophys Res-Ocean 1995;100:13321–32.
[93] Cota GF, Harrison WG, Platt T, et al. Bio-optical properties of the Labrador Sea. J Geophys Res-Ocean 2003;108:3228.
[94] Johnsen G, Sakshaug E. Biooptical characteristics of psii and psi in 33 species (13 pigment groups) of marine phytoplankton, and the relevance for pulse-amplitude-modulated and fast-repetition-rate fluorometry1. J Phycol 2010;43:1236–51.
[95] Campbell D, Hurry V, Clarke AK, et al. Chlorophyll fluorescence analysis of cyanobacterial photosynthesis and acclimation. Microbiol Mol Biol Res 1998;62:667.
[96] Simis SGH, Yannick H, Marcel B, et al. Optimization of variable fluorescence measurements of phytoplankton communities with cyanobacteria. Photosynth Res 2012;112:13–30.
[97] Seppälä J, Ylöstalo P, Kaitala S, et al. Ship-of-opportunity based phycocyanin fluorescence monitoring of the filamentous cyanobacteria bloom dynamics in the Baltic Sea. Estuar Coast Sci 2007;73:489–500.
[98] Cannizzaro JP, Carder KL, Chen FR, et al. A novel technique for detection of the toxic dinoflagellate, Karenia brevis, in the gulf of Mexico from remotely sensed ocean color data. Cont Shelf Res 2008;28:137–58.
[99] Gower JFR, Doerffer R, Borstad GA. Interpretation of the 685 nm peak in water-leaving radiance spectra in terms of fluorescence, absorption and scattering, and its observation by MERIS. Int J Remote Sens 1999;20:1771–86.
[100] Matthews MW, Odermatt D. Improved algorithm for routine monitoring of cyanobacteria and eutrophication in inland and near-coastal waters. Remote Sens Environ 2015;156:374–82.
[101] Gilerson A, Zhou J, Hlaing S, et al. Fluorescence component in the reflectance spectra from coastal waters. II. Performance of retrieval algorithms. Opt Express 2008;16:2446–60.
[102] Marion JW, Lee J, Lemeshow S, et al. *In vivo* phycocyanin flourometry as a potential rapid screening tool for predicting elevated microcystin concentrations at eutrophic lakes. Environ Sci Technol 2012;46:4523–31.
[103] Izydorczyk K, Carpentier C, Mrówczyński J, et al. Establishment of an alert level framework for cyanobacteria in drinking water resources by using the algae online analyser for monitoring cyanobacterial chlorophyll. Water Res 2009;43:989–96.
[104] Misra AN, Misra M, Singh R. Chlorophyll fluorescence in plant biology. Biophysics, Rijeka: In Tech; 2012. p. 171–92. 10.5772/35111.
[105] Genty B, Harbinson J, Briantais JM, et al. The relationship between non-photochemical quenching of chlorophyll fluorescence and the rate of photosystem 2 photochemistry in leaves. Photosynth Res 1990;25:249–57.
[106] Shi K, Shen H, Wang W, et al. Habitat-specific differences in adaptation to light in freshwater diatoms. J Appl Phycol 2016;28:1–13.
[107] White S, Anandraj A, Bux F. Pam fluorometry as a tool to assess microalgal nutrient stress and monitor cellular neutral lipids. Bioresour Technol 2011;102:1675–82.
[108] Dorigo U, Leboulanger C. A pulse-amplitude modulated fluorescence-based method for assessing the effects of photosystem ii herbicides on freshwater periphyton. J Appl Phycol 2001;13:509–15.
[109] Kalaji HM, Schansker G, Brestic M, et al. Frequently asked questions about chlorophyll fluorescence, the sequel. Photosynth Res 2017;132:13–66.
[110] Gregor J, Maršálek B, Šípková H. Detection and estimation of potentially toxic cyanobacteria in raw water at the drinking water treatment plant by *in vivo* fluorescence method. Water Res 2007;41:228–34.
[111] Kutser T. Passive optical remote sensing of cyanobacteria and other intense phytoplankton blooms in coastal and inland waters. Int J Remote Sens 2009;30:4401–25.
[112] Liang QC, Zhang YC, Ma RH, et al. A MODIS-based novel method to distinguish surface cyanobacterial scums and aquatic macrophytes in Lake Taihu. Remote Sens 2017;9:133.
[113] Matsushita B, Yang W, Yu G, et al. A hybrid algorithm for estimating the chlorophyll-*a* concentration across different trophic states in Asian inland waters. ISPRS J Photogr 2015;102:28–37.
[114] Qi L, Hu C, Duan H, et al. A novel MERIS algorithm to derive cyanobacterial phycocyanin pigment concentrations in a eutrophic lake: theoretical basis and practical considerations. Remote Sens Environ 2014;154:298–317.
[115] Kutser T, Metsamaa L, Strömbeck N, et al. Monitoring cyanobacterial blooms by satellite remote sensing. Estuar Coast Shelf Sci 2006;67:303–12.
[116] Woźniak M, Bradtke KM, Darecki M, et al. Empirical model for phycocyanin concentration estimation as an indicator of cyanobacterial bloom in the optically complex coastal waters of the Baltic Sea. Remote Sens 2016;8:212.
[117] Spyrakos E, O'Donnell R, Hunter PD, et al. Optical types of inland and coastal waters. Limnol Oceanogr 2018;63:846–70.
[118] Gower J, King S, Borstad G, et al. Detection of intense plankton blooms using the 709 nm band of the MERIS imaging spectrometer. Int J Remote Sens 2005;26:2005–12.
[119] Li YM, Qiao W, Wu CQ, et al. Estimation of chlorophyll *a* concentration using NIR/red bands of MERIS and classification procedure in inland turbid water. IEEE Trans Geosci Remote 2012;50:988–97.
[120] Duan HT, Ma RH, Zhang YC, et al. A new three-band algorithm for estimating chlorophyll concentrations in turbid inland lakes. Environ Res Lett 2010;5:044009.
[121] Fusilli L, Collins MO, Palombo A, et al. Assessment of the abnormal growth of floating macrophytes in winam Gulf (Kenya) by using MODIS imagery time series. Int J Appl Earth Obs 2013;20:33–41.
[122] Ogashawara I. Terminology and classification of bio-optical algorithms. Remote Sens Lett 2015;6:613–7.
[123] Gurlin D, Gitelson AA, Moses WJ. Remote estimation of chl-a concentration in turbid productive waters — return to a simple two-band NIR-red model? Remote Sens Environ 2011;115:3479–90.
[124] Ruddick KG, Gons HJ, Rijkeboer M, et al. Optical remote sensing of chlorophyll *a* in Case 2 waters by use of an adaptivetwo-band algorithm with optimal error properties. Appl Opt 2001;40:3575–85.
[125] Binding CE, Greenberg TA, Jerome JH, et al. An assessment of MERIS algal products during an intense bloom in lake of the woods. J Plankton Res 2011;33:793–806.
[126] Yacobi YZ, Moses WJ, Kaganovsky S, et al. NIR-red reflectance-based algorithms for chlorophyll-*a* estimation in mesotrophic inland and coastal waters: Lake Kinneret case study. Water Res 2011;45:2428–36.
[127] Dall'Olmo G, Gitelson AA, Rundquist DC, et al. Assessing the potential of SeaWiFS and MODIS for estimating chlorophyll concentration in turbid productive waters using red and near-infrared bands. Remote Sens Environ 2005;96:176–87.
[128] Moses WJ, Gitelson AA, Berdnikov S, et al. Estimation of chlorophyll-*a* concentration in Case II waters using MODIS and MERIS data—successes and challenges. Environ Res Lett 2009;4:045005.
[129] Tebbs EJ, Remedios JJ, Harper DM. Remote sensing of chlorophyll-*a* as a measure of cyanobacterial biomass in Lake Bogoria, a hypertrophic, saline-alkaline, flamingo lake, using Landsat ETM+. Remote Sens Environ 2013;135:92–106.

[130] Li Y, Zhang YL, Shi K, et al. Spatiotemporal dynamics of chlorophyll-*a* in a large reservoir as derived from Landsat 8 OLI data: understanding its driving and restrictive factors. Environ Sci Pollut Res 2018;25:1359–2137.
[131] Qi L, Hu CM, Duan HT, et al. An EOF-based algorithm to estimate chlorophyll *a* concentrations in Taihu Lake from MODIS land-band measurements: implications for near real-time applications and forecasting models. Remote Sens 2014;6:10694–715.
[132] Moses WJ, Saprygin V, Gerasyuk V, et al. OLCI-based NIR-red models for estimating chlorophyll-*a* concentration in productive coastal waters—a preliminary evaluation. Environ Res Comm 2019;1:011002.
[133] Koponen S, Pulliainen J, Kallio K, et al. Lake water quality classification with airborne hyperspectral spectrometer and simulated MERIS data. Remote Sens Environ 2002;79:51–9.
[134] Yacobi YZ, Gitelson A, Mayo M. Remote sensing of chlorophyll in Lake Kinneret using highspectral-resolution radiometer and Landsat TM: spectral features of reflectance and algorithm development. J Plankton Res 1995;17:2155–73.
[135] Gons HJ. Optical teledetection of chlorophyll *a* in turbid inland waters. Environ Sci Technol 1999;33:1127–32.
[136] Smith M, Robertson Lain L, Bernard S. An optimized chlorophyll *a* switching algorithm for MERIS and OLCI in phytoplankton-dominated waters. Remote Sens Environ 2018;215:217–27.
[137] Wheeler SM, Morrissey LA, Levine SN, et al. Mapping cyanobacterial blooms in lake champlain's missisquoi bay using Quickbird and MERIS satellite data. J Great Lakes Res 2012;38:68–75.
[138] Gitelson A. The peak near 700 nm on radiance spectra of algae and water: relationships of its magnitude and position with chlorophyll concentration. Int J Remote Sens 1992;13:3367–73.
[139] Le CF, Li YM, Zha Y, et al. Remote estimation of chlorophyll *a* in optically complex waters based on optical classification. Remote Sens Environ 2011;115:725–37.
[140] Shi K, Li YM, Li L, et al. Remote chlorophyll-*a* estimates for inland waters based on a cluster-based classification. Sci Total Environ 2013;444:1–15.
[141] Gons HJ, Rijkeboer M, Ruddick KG. Effect of a waveband shift on chlorophyll retrieval from MERIS imagery of inland and coastal waters. J Plankton Res 2005;27:125–7.
[142] Gower J. Observations of *in situ* fluorescence of chlorophyll-*a* in Saanich Inlet. Bound-Lay Meteorol 1980;13:235–45.
[143] Lee Z, Carder KL, Hawes SK, et al. Model for the interpretation of hyperspectral remote-sensing reflectance. Appl Opt 1994;33:5721–32.
[144] Gitelson AA, Gurlin D, Moses WJ, et al. A bio-optical algorithm for the remote estimation of the chlorophyll-aconcentration in Case 2 waters. Environ Res Lett 2009;4:045003.
[145] Ogashawara I, Mishra RD, Mishra S, et al. A performance review of reflectance based algorithms for predicting phycocyanin concentrations in inland waters. Remote Sens 2013;5:4774–98.
[146] Pyo CJ, Ligaray M, Kwon SY, et al. High-spatial resolution monitoring of phycocyanin and chlorophyll-*a* using airborne hyperspectral imagery. Remote Sens 2018;10:1180.
[147] Tao M, Duan HT, Cao ZG, et al. A hybrid eof algorithm to improve MODIS cyanobacteria phycocyanin data quality in a highly turbid lake: bloom and nonbloom condition. IEEE J-STARS 2017;10:4430–44.
[148] Mishra S, Mishra RD, Schluchter MW. A novel algorithm for predicting phycocyanin concentrations in cyanobacteria: a proximal hyperspectral remote sensing approach. Remote Sens 2009;1:758–75.
[149] Hunter PD, Tyler AN, Willby NJ, et al. The spatial dynamics of vertical migration by microcystis aeruginosa in a eutrophic shallow lake: a case study using high spatial resolution time-series airborne remote sensing. Limnol Oceanogr 2008;53:2391–406.
[150] Schalles J, Yacobi Y. Remote detection and seasonal patterns of phycocyanin, carotenoid and chlorophyll pigments in eutrophic waters. Arch Hydrobiol 2000;55:153–68.
[151] Dash P, Walker ND, Mishra DR, et al. Estimation of cyanobacterial pigments in a freshwater lake using OCM satellite data. Remote Sens Environ 2011;115:3409–23.
[152] Gomez JAD, Alonso CA, Garcia AA. Remote sensing as a tool for monitoring water quality parameters for mediterranean lakes of european union water framework directive (WFD) and as a system of surveillance of cyanobacterial harmful algae blooms (scyanohabs). Environ Monit Assess 2011;181:317–34.
[153] Soja-Woźniak M, Craig ES, Kratzer S, et al. A novel statistical approach for ocean colour estimation of inherent optical properties and cyanobacteria abundance in optically complex waters. Remote Sens 2017;9:343.
[154] Zhang YC, Ma RH, Duan HT, et al. A novel algorithm to estimate algal bloom coverage to subpixel resolution in Lake Taihu. IEEE J-STARS 2014;7:3060–8.
[155] Carvalho GA, Minnett PJ, Fleming LE, et al. Satellite remote sensing of harmful algal blooms: a new multi-algorithm method for detecting the Florida Red tide (Karenia Brevis). Harmful Algae 2010;9:440–8.
[156] Gower JFR. Red tide monitoring using AVHRR HRPT imagery from a local receiver. Remote Sens Environ 1994;48:309–18.
[157] Shanmugam P, Ahn YH, Ram PS. SeaWiFS sensing of hazardous algal blooms and their underlying mechanisms in shelf-slope waters of the Northwest Pacific during summer. Remote Sens Environ 2008;112:3248–70.
[158] Hu CM. A novel ocean color index to detect floating algae in the global oceans. Remote Sens Environ 2009;113:2118–29.
[159] Chen X, Shang SL, Lee ZP, et al. High-frequency observation of floating algae from AHI on Himawari-8. Remote Sens Environ 2019;227:151–61.
[160] Liu XH, Zhang YL, Shi K, et al. Mapping aquatic vegetation in a large, shallow eutrophic lake: a frequency-based approach using multiple years of MODIS data. Remote Sens 2015;7:10295–320.
[161] Zhang YC, Ma RH, Zhang M, et al. Fourteen-year record (2000–2013) of the spatial and temporal dynamics of floating algae blooms in Lake Chaohu, observed from time series of MODIS images. Remote Sens 2015;7:10523–42.
[162] Huang CC, Li YM, Yang H, et al. Detection of algal bloom and factors influencing its formation in Taihu Lake from 2000 to 2011 by MODIS. Environ Earth Sci 2014;71:3705–14.
[163] Duan HT, Loiselle SA, Zhu L, et al. Distribution and incidence of algal blooms in Lake Taihu. Aquat Sci 2015;77:9–16.
[164] Fang C, Song KS, Li L, et al. Spatial variability and temporal dynamics of habs in Northeast China. Ecol Indic 2018;90:280–94.
[165] Mu M, Wu CQ, Li YM, et al. Long-term observation of cyanobacteria blooms using multi-source satellite images: a case study on a cloudy and rainy lake. Environ Sci Pollut R 2019;26:11012–28.
[166] Huang CC, Wang X, Yang H, et al. Satellite data regarding the eutrophication response to human activities in the plateau Lake Dianchi in China from 1974 to 2009. Sci Total Environ 2014;485–486:1–11.
[167] Xing QG, Hu CM. Mapping macroalgal blooms in the Yellow Sea and East China sea using HJ-1 and Landsat data: application of a virtual baseline reflectance height technique. Remote Sens Environ 2016;178:113–26.
[168] Fang C, Song KS, Shang Y, et al. Remote sensing of harmful algal blooms variability for Lake Hulun using adjusted FAI (AFAI) algorithm. Environl Inform 2018:54–68.
[169] Wynne TT, Stumpf RP, Briggs TO. Comparing MODIS and MERIS spectral shapes for cyanobacterial bloom detection. Int J Remote Sens 2013;34:6668–78.
[170] Olmanson LG, Bauer ME, Brezonik PL. A 20-year Landsat water clarity census of Minnesota's 10000 lakes. Remote Sens Environ 2008;112:4086–97.
[171] Stumpf RP, Wynne TT, Baker DB, et al. Interannual variability of cyanobacterial blooms in Lake Erie. PLoS One 2012;7:e42444.
[172] Bonansea M, Rodriguez MC, Pinotti L, et al. Using multi-temporal Landsat imagery and linear mixed models for assessing water quality parameters in Río Tercero Reservoir (Argentina). Remote Sens Environ 2015;158:28–41.
[173] Bresciani M, Cazzaniga I, Austoni M, et al. Mapping phytoplankton blooms in deep subalpine lakes from Sentinel-2A and Landsat-8. Hydrobiologia 2018;824:197–214.
[174] Watanabe FSY, Alcantara E, Rodrigues TWP, et al. Estimation of chlorophyll-*a* concentration and the trophic state of the Barra Bonita hydroelectric reservoir using OLI/Landsat-8 images. Int J Env Res Pub He 2015;12:10391–417.
[175] Ho JC, Stumpf RP, Bridgeman TB, et al. Using Landsat to extend the historical record of lacustrine phytoplankton blooms: a Lake Erie case study. Remote Sens Environ 2017;191:273–85.
[176] Huang CC, Zhang YL, Huang T, et al. Long-term variation of phytoplankton biomass and physiology in Taihu Lake as observed via MODIS satellite. Water Res 2019;153:187–99.
[177] Binding CE, Greenberg TA, Bukata RP. An analysis of MDOSI-derived algal and mineral turbidity in Lake Erie. J Great Lakes Res 2012;38:107–16.
[178] Shi K, Zhang YL, Zhang YB, et al. Phenology of phytoplankton blooms in a trophic lake observed from long-term MODIS data. Environ Sci Technol 2019;53:2324–31.
[179] Chaffin JD, Mishra S, Kane DD, et al. Cyanobacterial blooms in the central basin of Lake Erie: Potentials for cyanotoxins and environmental drivers. J Great Lakes Res 2019;45:277–89.
[180] Becker RH, Sultan MI, Boyer GL, et al. Mapping cyanobacterial blooms in the great lakes using MODIS. J Great Lakes Res 2009;35:447–53.
[181] Horion S, Bergamino N, Stenuite S, et al. Optimized extraction of daily bio-optical time series derived from MODIS/Aqua imagery for Lake Tanganyika, Africa. Remote Sens Environ 2010;114:781–91.
[182] Matthews MW. Eutrophication and cyanobacterial blooms in South African inland waters: 10 years of MERIS observations. Remote Sens Environ 2014;155:161–77.
[183] Bresciani M, Adamo M, De Carolis G, et al. Monitoring blooms and surface accumulation of cyanobacteria in the curonian lagoon by combining MERIS and ASAR data. Remote Sens Environ 2014;146:124–35.
[184] Feng L, Hu CM, Han XX, et al. Long-term distribution patterns of chlorophyll-*a* concentration in China's largest freshwater lake: MERIS full-resolution observations with a practical approach. Remote Sens 2015;7:275–99.

Kun Shi is an associate professor in Nanjing Institute of Geography and Limnology, Chinese Academy of Sciences. His research interests include water optics, water color remote sensing, ecological effects of changes in lake environment.

Yunlin Zhang is a professor in Nanjing Institute of Geography and Limnology, Chinese Academy of Sciences. His study interests include lake optics and water color remote sensing, lakes thermodynamics, and chromophoric dissolved organic matter (CDOM) biogeochemistry cycle.